

# **Forschungszentrum Karlsruhe**

Technik und Umwelt

Wissenschaftliche Berichte

FZKA 6656

## **Criteria for the Spreading of Oxide Melts: Test Series miniKATS-1 to -5**

B. Eppinger, G. Fieg, H. Massier, W. Schütz, U. Stegmaier  
G. Stern\*

Institut für Kern- und Energietechnik

Institut für Hochleistungsimpuls- und Mikrowellentechnik

Institut für Reaktorsicherheit

Institut für Materialforschung

Programm Nukleare Sicherheitsforschung

\*Firma Pro Science, Ettlingen

Forschungszentrum Karlsruhe GmbH, Karlsruhe

2001

**Impressum der Print-Ausgabe:**

**Als Manuskript gedruckt  
Für diesen Bericht behalten wir uns alle Rechte vor**

**Forschungszentrum Karlsruhe GmbH  
Postfach 3640, 76021 Karlsruhe**

**Mitglied der Hermann von Helmholtz-Gemeinschaft  
Deutscher Forschungszentren (HGF)**

**ISSN 0947-8620**

# Zusammenfassung

## Kriterien zur Ausbreitung oxidischer Schmelzen:

### Die Tests miniKATS-1 bis -5

In einer großangelegten Serie von Tests zur Ausbreitung oxidischer Hochtemperaturschmelzen in einem größeren Maßstab (KATS-Tests) wurden Parameter variiert, die das Ausbreitungsverhalten der Schmelze wesentlich beeinflussen (Viskosität, Volumenrate der Schmelze, Substratum der Ausbreitungsfläche, Gegenwart von Wasser). Trotz einer umfangreichen Instrumentierung mit Thermoelementen verschiedener Art, einer Infrarotkamera und mehreren Videokameras konnte nur in wenigen Fällen das Verhalten der Schmelze an der vordersten Front im Augenblick des Stillstands detailliert untersucht werden. Mit der miniKATS-Serie wurden deshalb fünf weitere Ausbreitungstest mit oxidischen Schmelzen in kleinem Maßstab (ca. 5 kg) durchgeführt, bei denen die vorderste Front im Augenblick des Stillstandes auf ihre mechanischen Eigenschaften untersucht wurde. Es stellte sich dabei heraus, dass in allen Fällen der bulk-Bereich der Schmelze im flüssigen Zustand bei nahezu Anfangstemperatur angefundene wurde. Je nach Beschaffenheit der Anfangsschmelze wurde die Ausbreitung durch zwei unterschiedliche Phänomene am weiteren Ausbreiten behindert: durch Krustenbildung an der Oberfläche, in diesem Falle vereinigten sich die Krusten am Boden mit der, die sich an der Oberfläche bildete. In den anderen Fällen war die gesamte Schmelzenzunge im noch flüssigen Zustand oberhalb der Liquidus-Temperatur als die Ausbreitung gestoppt wurde. Hier spielte die Oberflächenspannung eine dominierende Rolle, sie stand im Gleichgewicht mit der Schwerkraft als treibende Kraft. In keinem der Fälle konnte „bulk-freezing“ nachgewiesen werden.

## Abstract

In a long series of larger spreading tests with high temperature oxide melts (KATS tests) many parameters have been varied which are influencing the spreading behaviour (viscosity, pouring rate, substratum of spreading surface, presence of water). In spite of an extensive instrumentation using different thermocouples, an infrared camera and several video cameras, only in very few cases the behaviour of the melt front at the very moment of immobilization could be detected in detail. Therefore in the additional miniKATS series five small scale (5 kg) spreading tests with oxide melts have been conducted to investigate the mechanical properties of the spreading front in the moment of immobilization. It turned out that in all cases the bulk of the melt at this moment was still liquid at a temperature close to the initial one. Depending on the initial melt properties two distinct phenomena have been observed which control the immobilization of the melt: the first phenomena is the crust formation at the surface, the crusts at the bottom combined with the crust at the surface of the melt. In the other case the whole melt front was still above the liquid temperature at the moment of immobilization. Here the surface tension was controlling the spreading, it was in balance with the driving gravitational force. In none of the test bulk freezing has been detected.

# Table of contents

1	Introduction	1
2	Spreading behaviour of high-temperature oxide melts .....	3
3	Experiments .....	5
3.1	Test facility .....	5
3.2	Instrumentation and data recording.....	7
3.3	Test performance .....	8
3.4	Melt characteristics.....	9
3.5	Pouring rates.....	11
4	Description of observed spreading behaviour .....	13
4.1	miniKATS-1 .....	16
4.1.1	Details of the spreading process (see Figure 6, Figure 7 and Table 3)....	16
4.1.2	Post-test examination .....	20
4.1.3	Summary.....	20
4.2	miniKATS-2 .....	21
4.2.1	Details of the spreading process (Figure 6 and Figure 8) .....	22
4.2.2	Post-test examination .....	25
4.2.3	Summary.....	26
4.3	miniKATS-3.....	27
4.3.1	Details of the spreading process.....	27
4.3.2	Post-test examination .....	28
4.4	miniKATS-4 .....	29
4.4.1	Details of the spreading process (Figure 6 and Figure 10) .....	29
4.4.2	Post-test examination .....	32
4.4.3	Summary.....	32
4.5	miniKATS-5.....	33
4.5.1	Details of the spreading process (Figure 6, Figure 11 to Figure 15) .....	33
4.5.2	Post-test examination .....	37
4.5.3	Summary.....	38

5	Discussion of observed spreading behaviour .....	38
5.1	Spreading of strongly superheated melts (miniKATS-2 to -5).....	38
5.2	Spreading of melts with temperatures near the liquidus temperature (miniKATS-1).....	40
5.3	Comparison of spreading behaviour in miniKATS-2 to -5, miniKATS-1 and the large KATS tests .....	43
6	Conclusions.....	44
7	Literatur .....	45

## List of Figures

Figure 1: Concept of the EPR core catcher	1
Figure 2: Balances of driving and retarding pressures of a spreading melt	4
Figure 3: Experimental Setup of the miniKATS tests	5
Figure 4: GEMINI results for the solid mass fraction in the solidus-liquidus range	11
Figure 5: Calculated pouring rates and melt level of the finally spread melt in the miniKATS tests	13
Figure 6: Transient spreading of oxide melt in miniKATS. Calculated volumetric flow rate is added.	15
Figure 7: Melt surface infrared pictures in miniKATS-1 at different times	18
Figure 8: Melt surface infrared pictures in miniKATS-2 at different times	24
Figure 9: Cross-section of the solidified melt after the test	26
Figure 10: Melt surface infrared pictures in miniKATS-4 at different times	31
Figure 11: Melt surface infrared pictures in miniKATS-5 at different times	34
Figure 12: Melt surface photo in miniKATS-5 at 5.9 s after start of spreading	36
Figure 13: Melt surface photo in miniKATS-5 at 6.8 s after start of spreading	36
Figure 14: Melt surface photos in miniKATS-5 at 8.6 s after start of spreading	36
Figure 15: Shape of the solidified melt after the test	37
Figure 16: Calculated transient melt heights in tests miniKATS-2 to -5	39
Figure 17: Calculated transient melt heights in miniKATS-1	41

## List of Tables

Table 1: Initial and boundary conditions for spreading	6
Table 2: Masses and compositions of melts	9
Table 3: Melt characteristics	10
Table 4: Comparison of the melt front bulk temperature at immobilisation to the initial temperature	42



# 1 Introduction

Next generation Light Water Reactors shall, in the case of a core meltdown accident, incorporate the ability to retain the core melt within the containment to exclude significant radioactive release to the environment. In the case of the European Pressurized Water Reactor (EPR), an ex-vessel core catcher is foreseen to meet the requirements, Figure 1 [1] [2]. The core melt is firstly collected temporarily (~1 h) in the reactor cavity below the reactor pressure vessel. In the reactor cavity the core melt interacts with sacrificial concrete. At the end of the melt-concrete interaction (MCCI) a melt gate (melt plug) at the bottom will be eroded and the corium melt is released to spread on a prepared area (~170 m<sup>2</sup>) where it will be flooded by water to extract the decay heat and to solidify.

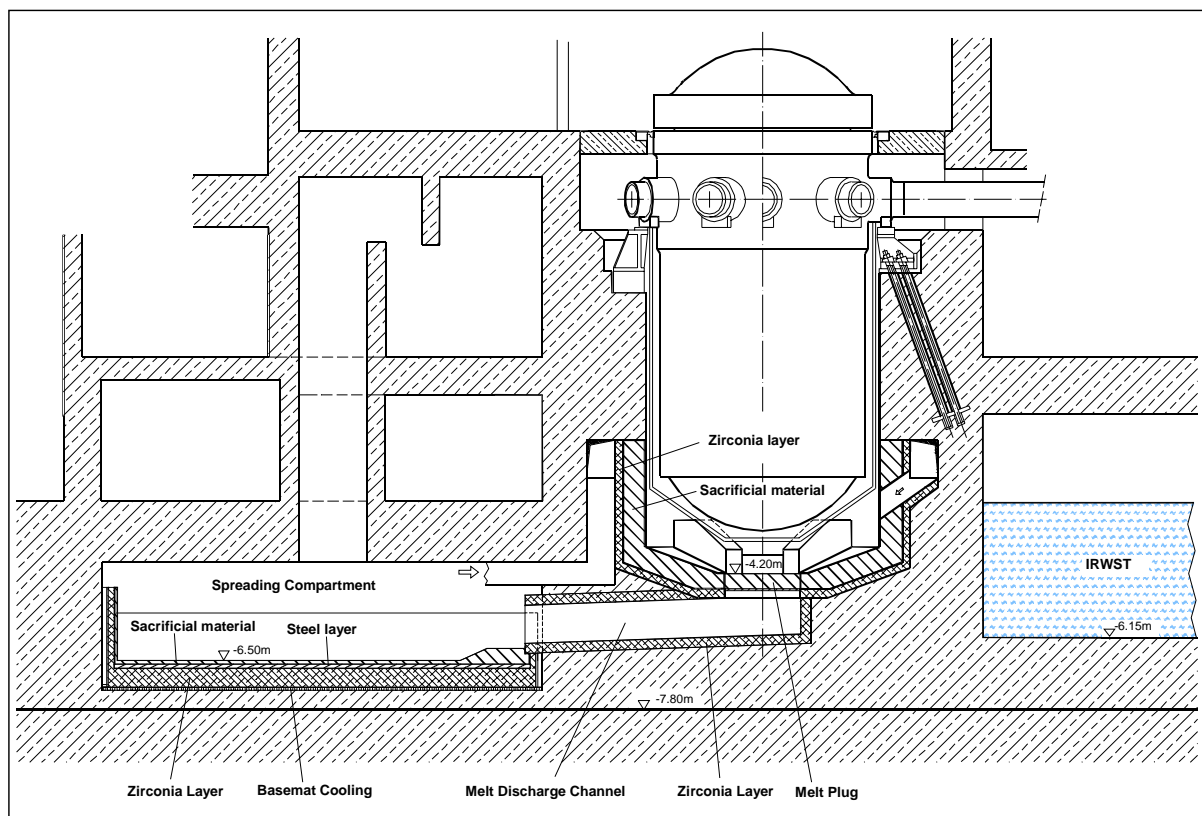


Figure 1: Concept of the EPR core catcher

It is important for this concept that the melt spreads rather homogeneously over the spreading area. To prove this, computer codes, for example the CORFLOW code from Siemens [3] [4] and the THEMA code in France [5], are developed to describe

the spreading behaviour and large-scale spreading tests are performed at different laboratories to verify these codes.

At the Forschungszentrum Karlsruhe large-scale spreading tests [6] [7] with iron and alumina melts, generated by the thermite reaction, are performed. To achieve EPR representative oxide melts ( $\text{UO}_2/\text{ZrO}_2$  + eroded sacrificial concrete), which are characterised by a large difference between the solidus and liquidus temperatures, other oxides ( $\text{SiO}_2$ ,  $\text{FeO}$ ) are added to the alumina melt.

Oxide melt spreading is a key problem of the EPR-concept and has therefore been studied in a series of KATS tests. Nevertheless, because the oxide spreading is so complex, the details are still not completely understood and especially it is still not clear, which of the possible effects (surface tension, high viscosity, crust formation) finally causes stop of spreading. To clear these questions, accompanying to the large KATS tests, a series of well-instrumented small-scale tests (miniKATS) with oxide melts (about 5 – 10 kg) have been performed. The observation was concentrated on crust formation and on the phenomena at the melt front, because these are considered to be especially important for the stop of spreading.

In the present report, after a short description of the problem, parameters, results and interpretation of a series of five experiments will be presented.

## 2 Spreading behaviour of high-temperature oxide melts

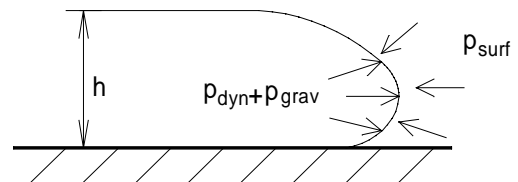
Even the isothermal spreading of a non-freezing liquid is, in the case of incomplete wetting, finally limited by the surface tension. In this work high temperature melts composed of different oxides are considered. These melts are characterised by a solidus temperature of  $\sim 1600^{\circ}\text{C}$  and a liquidus temperature in the range of  $1850$  to  $2050^{\circ}\text{C}$ . For such melts the spreading may also be limited by local freezing (crust formation) or bulk freezing and/or by a steep increase of viscosity, which is caused by a decrease of the melt temperature during spreading. The miniKATS melts are considered to be Newtonian, for Non-Newtonian fluids other effects may cause a stop of spreading.

In any case, the maximum possible spreading (corresponding to a minimum height  $h_{\min}$  of the spread melt) is determined by surface tension.

Driving forces for the spreading are the dynamical and the gravitational pressure. As in the miniKATS experiments the spreading surface is horizontal, the gravitational pressure is determined by the height of the melt slug itself

Gravitational pressure:  $p_{grav} = \rho \cdot g \cdot h$

Dynamical pressure:  $p_{dyn} = \frac{\rho}{2} \cdot v^2$



Surface tension pressure:  $p_{surf} = \frac{2 \cdot \sigma}{r}$

With:

$h$  = melt height

$r = h / 2$  = curvature radius at the front

$\sigma$  = surface tension  $\sigma = 0.6 \text{ N/m}$  (for alumina)

$\rho$  = specific density

$v$  = velocity of the melt front

Assuming that the leading edge of the spreading melt mass is not influenced by crusts, the equilibrium of  $p_{\text{dyn}}$ ,  $p_{\text{grav}}$  and  $p_{\text{surf}}$  stops the melt. At the time of melt stop the spreading velocity (and the dynamic pressure) is zero and the minimum height of the spread melt is given by

$$h_{\text{min}} = \sqrt{\frac{4 \cdot \sigma}{\rho \cdot g}}$$

Figure 2 shows  $p_{\text{grav}}$  and  $p_{\text{surf}}$  in dependence on the melt height  $h$  and, to get an impression of the order of magnitude, also  $p_{\text{dyn}}$  in dependence on the spreading velocity  $v$ .

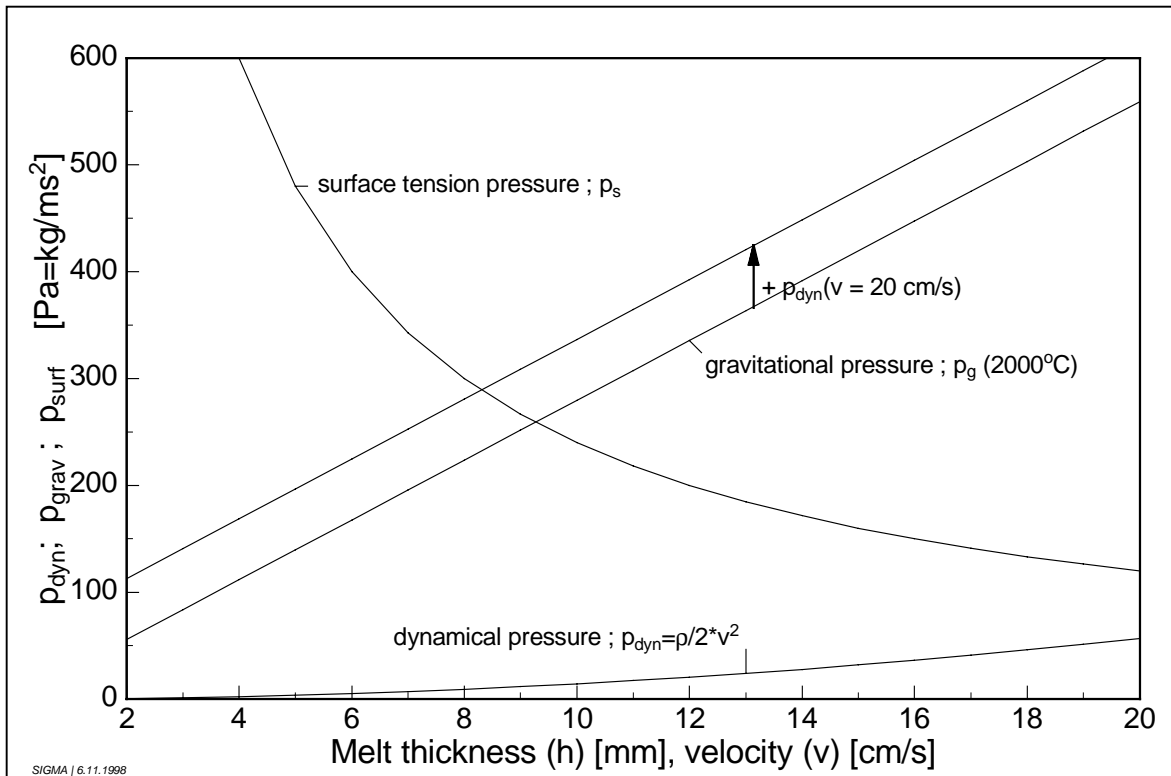


Figure 2: Balances of driving and retarding pressures of a spreading melt

The point of intersection of the curve of  $p_{\text{grav}}$  and the surface tension curve of  $p_s$  gives the minimum melt slug thickness. At a melt temperature of 2000°C, the density of a typical oxide miniKATS oxide melt is  $\rho = 2850 \text{ kg/m}^3$ , which leads to a resulting melt height of  $h_{\text{min}} = 9.3 \text{ mm}$ . At a melt temperature of 2130°C the density is  $\rho = 2720 \text{ kg/m}^3$  which leads to a resulting melt height of  $h_{\text{min}} = 9.5 \text{ mm}$ .

The dynamic pressure causes at most a temporary overshooting of the spreading length with a decrease of spreading height. But, as can be seen from the diagram above, this effect is small. Assuming a quite high velocity of 20 cm/s the melt height is reduced only by ~1 mm.

### 3 Experiments

#### 3.1 Test facility

The experimental setup, Figure 3, consists of three main components: a small reaction crucible, a swamp volume to separate the iron melt from the oxide melt and the spreading channel (steel) on which the oxide melt is spread.

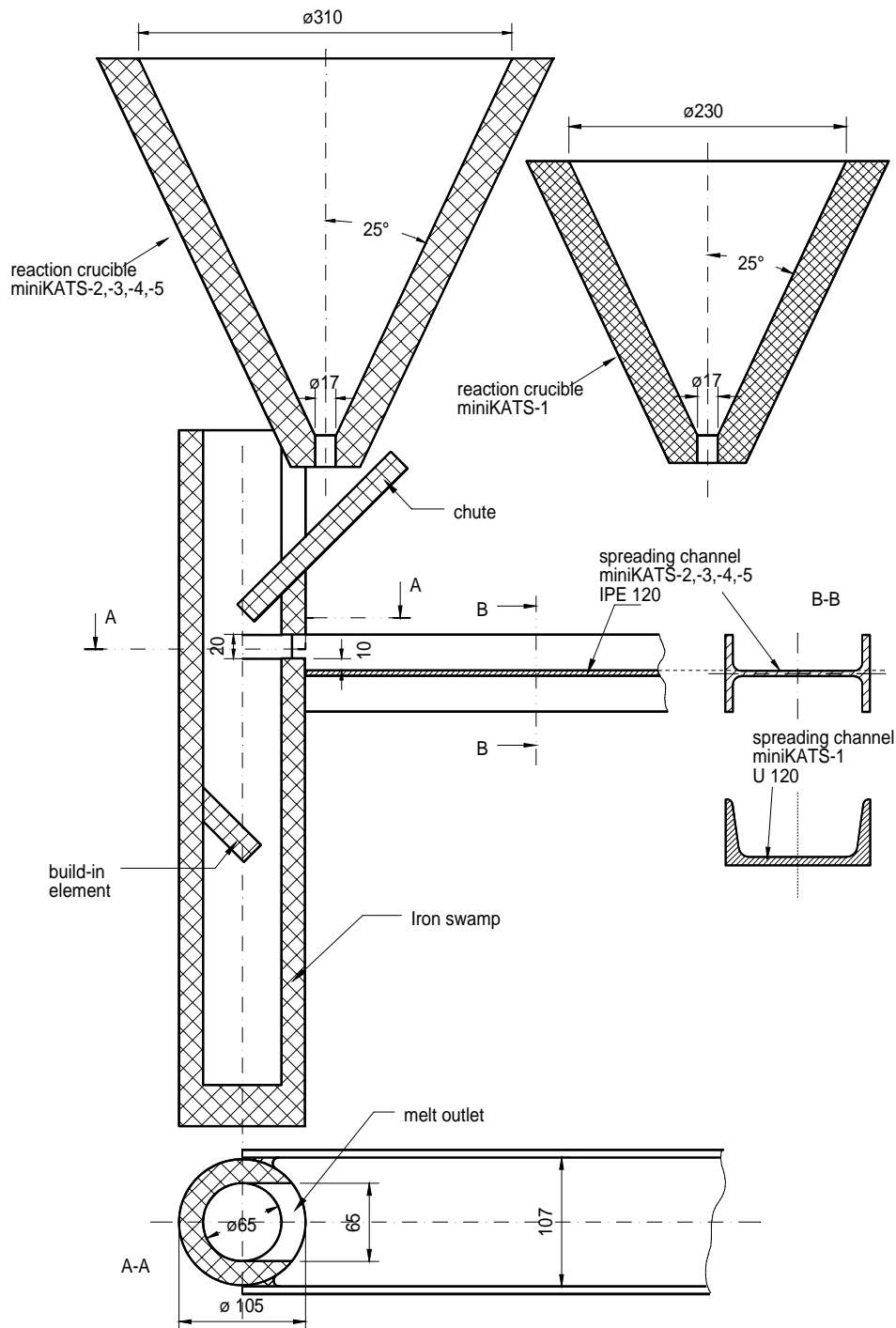


Figure 3: Experimental Setup of the miniKATS tests

During the performance of the experiments miniKATS-1 to –5 parts of this setup have been changed and improved. Since miniKATS-2 a slightly larger crucible with a different protective lining material has been used. The spreading channel was made of steel and has been changed from a U-shaped to a double T-profile in order to reduce bowing by the spread hot melt (bowing occurs after immobilization of the melt). Important improvements have been made concerning the melt flow from the crucible into the swamp. Since miniKATS-2 the melt flows more gently over an inclined chute into the swamp and after miniKATS-3 build-in elements inside the swamp volume were added to calm down the flow and prevent direct transfer of melt from the reaction crucible to the spreading channel. By these provisions the amount of iron on the spreading channel of miniKATS-4 and -5 was very small, while in miniKATS-1 to -3 it was between 0.6 and 1.8 kg iron. For miniKATS-5 a smaller swamp cylinder was used but with the same volume as in miniKATS-4 (data of swamp volumes are given in Table 1.)

Table 1: Initial and boundary conditions for spreading

		miniKATS-1	miniKATS-2	miniKATS-3	miniKATS-4	miniKATS-5
Channel material		Steel	Steel	Steel	Steel	Steel
Channel width		102 mm	107 mm	107 mm	107 mm	107 mm
Swamp volume		$\varnothing 65 \times 316$ = 1.05 dm <sup>3</sup>	$\varnothing 65 \times 340$ = 1.13 dm <sup>3</sup>	$\varnothing 65 \times 355$ = 1.18 dm <sup>3</sup>	$\varnothing 65 \times 355$ = 1.18 dm <sup>3</sup>	$\varnothing 45 \times 740$ = 1.18 dm <sup>3</sup>
Spread masses	Iron	~ 1 kg	0.58 kg	1.80 kg	0.1 kg	0 kg
	Oxide	4.32 kg	5.14 kg	5.71 kg	5.44 kg	5.62 kg
Initial temperature		2015°C	>> 2130°C	≥ 2130°C	≥ 2130°C	≥ 2130°C
Pouring duration	Calculated	5.6 s	6.2 s	7.2 s	6.3 s	6.3 s
	Observed	Not visible	Not visible	~7 s	~6 s	~5.9 s
Pouring rate (initial)	Calculated	0.38 l/s	0.39 l/s	0.40 l/s	0.39 l/s	0.39 l/s

The reaction crucible used for miniKATS-1 had a lining material of alumina based ceramic material, the crucible that was used in the further experiments had a ceramic lining consisting mainly of magnesia which turned out to be more resistant against the thermal attack during the thermite reaction. The geometry of both crucibles is shown in Figure 3. The nozzle diameter of the crucibles is 17 mm. From the crucible geometry, the melt level in the crucible and the nozzle diameter the volumetric flow rate for spreading is calculated (Section 3.5). Before conduct of the experiment the nozzle is closed by several metal foil layers and synthetic material, which is covered with a special type of sand to keep the thermite from melting the foil too early. This method gives a short delay time to ensure completion of the thermite reaction and separation of the two melt phases. The iron swamp is made of cordierite cylinders of 65 or 45 mm diameter, Table 1. Cordierite is a ceramic consisting of 47 %  $\text{SiO}_2$ , 45 %  $\text{Al}_2\text{O}_3$  and 6 %  $\text{MgO}$ . The volume is large enough to gather all the iron and some amount of oxide. After the volume is filled up, the melt flows through an orifice in the upper part of the swamp cylinder and over a small dam (~10 mm high) to spread on the channel. The channels are of usual structural steel (St 37) with U- or IPE-profile (double T): U-profile DIN 1026 – St 37 – U 120; IPE-profile DIN 1025 – St 37 – IPE 120, Figure 3.

### **3.2 Instrumentation and data recording**

The whole course of events during conduct of the tests is recorded by video cameras. Three video cameras are used for detailed recording of the spreading process, they are positioned 4 m above the spreading channel on a scaffolding. From miniKATS-3 on this recording was improved by the use of optical filters, which enabled a better observation of the structures on the surface of the spreading melt. In addition, an infrared camera is used in all tests to determine the surface temperature of the spreading melt. No other instrumentation for temperature measurements has been employed due to the good experience of infrared surface temperature measurements in the preceding KATS tests. In the tests miniKATS-1 to – 4 the infrared camera was placed at the same position as the video cameras. In miniKATS-5 the position of the infrared camera was lowered so that it was more focussed towards the end of the channel. This was done to get more information on the flow behaviour near the leading edge. In addition a photo camera with motor winder (up to 4 frames per second)

was used in miniKATS-4 and -5 to document the most interesting phases of the spreading process. For synchronisation of the different video recordings a flashlight is triggered together with the command for thermite ignition and start of the PC-recording of the infrared camera.

### **3.3 Test performance**

The thermite powder to produce the high temperature oxide melt is a stoichiometric mixture of  $\text{Fe}_2\text{O}_3$ ,  $\text{Fe}_3\text{O}_4$  and aluminum powder with an additional charge of 3 wt% aluminum to compensate for possible losses due to evaporation. In the first two tests miniKATS-1 and miniKATS-2, the reaction crucible was filled with 10.4 kg respectively with 10.9 kg of this thermite mixture. In the tests miniKATS-3 to -5 quartz sand (0.7 kg) was added to the 11 kg thermite powder to get an oxide phase with a  $\text{SiO}_2$ -content of about 10 wt%. With this additional oxide both, the liquidus and the solidus temperatures of the melt are lowered and, more important, the solidus-liquidus range is enlarged. This is done for a better simulation of a corium melt, which is characterized by a large solidus-liquidus temperature range.

The time between ignition and opening of the nozzle was ~40 s in miniKATS-1. In miniKATS-2 this time was much shorter, only ~20 s, the reason for this is unknown. The addition of quartz sand in miniKATS-3 to -5 leads again to longer periods of about 30 s (Table 2). When the nozzle opens, the denser iron melt is first released from the crucible into the swamp volume below. As described above, the use of a chute and additional build-in elements in the swamp prevented the iron melt from spreading onto the channel. It takes about 2 or 3 seconds until the swamp volume is filled, and the oxide melt finally flows over the small dam and spreads onto the channel. The pouring time lasts for about 6 to 7 s. Pouring duration and volumetric flow rate are calculated in Section 3.5. Spreading does not stop with the end of pouring, it continues on for a few more seconds. When spreading finally comes to an end, in some of the tests the oxide crust at the leading edge was immediately cut mechanically with a sort of a hatchet to check if further spreading would occur. The effects that were seen in each test are described in detail in Section 4.

Table 2: Masses and compositions of melts

		miniKATS-1	miniKATS-2	MiniKATS-3	miniKATS-4	miniKATS-5
Date		1.10.97	3.11.97	Nov. 97	3.12.97	4.2.98
Input	Thermite	10.4 kg	10.9 kg	11.0 kg	11.0 kg	11.0 kg
	Sand	0 kg	0 kg	0.7 kg	0.7 kg	0.7 kg
Output (weighed)	Iron (total)	4.72 kg	5.12 kg	5.02 kg	5.12 kg	5.18 kg
	Oxide (total)	5.19 kg	6.31 kg	6.78 kg	6.74 kg	?
Oxide composition (Analysed by IMF I. Chemische Analytik)	Al <sub>2</sub> O <sub>3</sub>	92.5 %	81.5 %	76.1 %	77.2 %	77.1 %
	FeO	5.4 %	5.2 %	9.9 %	10.8 %	11.1 %
	SiO <sub>2</sub>	1.9 %	2.5 %	8.4 %	8.7 %	7.8 %
	MgO	<0.1 %	10.3 %	3.7 %	2.3 %	2.5 %
Time between ignition and start of spreading		41.36 s	19.50 s	29.72 s	30.72 s	32.96 s

### 3.4 Melt characteristics

The oxide composition has been analysed after conduct of the tests [8]. The results are given in Table 2. Based on this post-test analysis, the solidus and liquidus temperatures as well as the liquid fraction in the solidus-liquidus two-phase region have been calculated with the GEMINI code [9] (Figure 4, Table 3). In most correlations which are used to evaluate the viscosity within this two-phase region, the viscosity increases so steeply below the temperature where the liquid fraction of the mixture drops below ~50 wt% ( $T_{50\%}$ , Table 3), that further spreading is essentially prevented. The two characteristic temperatures, which are important in terms of spreading, are quite different for the various melts: in miniKATS-1,  $T_{50\%}$  and  $T_{\text{liquidus}}$  are much higher (1950 and 2050°C, respectively) than in the other tests (~1700 and 1900°C, respectively).

Table 3: Melt characteristics

		miniKATS-1	miniKATS-2	miniKATS-3	miniKATS-4	miniKATS-5
$T_{liq}$ (°C) GEMINI-calculation		$\leq 2050^{\circ}\text{C}$	$\leq 1850^{\circ}\text{C}$	$\leq 1900^{\circ}\text{C}$		
$T_{sol}$ (°C) GEMINI-calculation		$\sim 1600^{\circ}\text{C}$	$\sim 1600^{\circ}\text{C}$	$\sim 1600^{\circ}\text{C}$		
$T_{50\%}$ (°C) GEMINI-calc.		$\sim 1950^{\circ}\text{C}$	$\sim 1760^{\circ}\text{C}$	$\sim 1670^{\circ}\text{C}$		
$T_{crust}$ (°C) experimental obs.		1935-1950°C	1880-1900°C	1780-1800°C		
$T_{initial}$ (°C)		2015°C	$\gg 2130^{\circ}\text{C}$	$\geq 2130^{\circ}\text{C}$	$\geq 2130^{\circ}\text{C}$	$\geq 2130$
Floating crust (earliest observation)	Time (s)	2.9 s	2.9 s	Not analysed	4 s	$\sim 5$ s
	Length (m)	0.4 / 0.5 m	1.0 m	"	1.25 m	1.6 m
	T (°C)	1935–1950°C	1880-1900°C	"	1780-1800°C	$\sim 1750^{\circ}\text{C}$
Sticking crust	Time (s)	3.8 / 3.7 s	5.6 s	"	6.9 s	7.2 s
	Length (m)	0.45 / 0.6 m	1.7 m	"	1.75 m	2.0 m
	T (°C)	1870-1890°C	1820-1830°C	"	$\sim 1650^{\circ}\text{C}$	1680–1700°C
Pouring duration	Calculated	5.6 s	6.2 s	7.2 s	6.3 s	6.3 s
	Observed	Not visible	Not visible	$\sim 7$ s	$\sim 6$ s	$\sim 5.9$ s
End spreading whole width / single tongue	Time (s)	9.4 s	7.5 s	10.4 / 13.4 s	9.5 / 15.9 s	7.2 / 9.6 s
	Length (m)	1.08 m	1.86 m	2.0 / 1.97 m	1.85 / 2.0 m	2.0 / 2.22 m
	$T_{max}$ (°C)	1990°C (1.0m)	1900°C (1.8m)	1790°C (1.9m)	1800°C (1.8m) 1790°C (2.0m)	1700°C (2.0m)
Hatchet	Time (s)	12.5 s	9.0 s	-	15.9 s	12 s
	Further spreading (m)	1.28 m	?	-	2.03 m	No
	Final stop (s)	16 s	?	-	17.3 s	-
	$T_{bulk}$ (°C)	1970–1980°C	2100°C	-	1830°C	2000°C

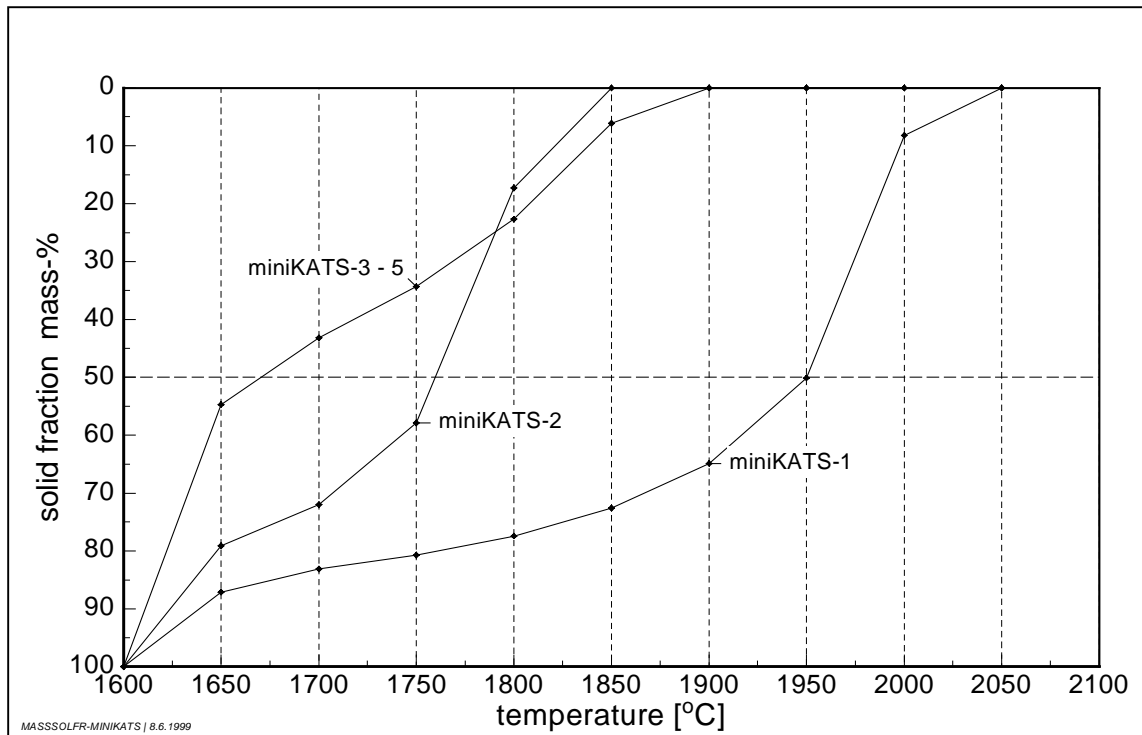


Figure 4: GEMINI results for the solid mass fraction in the solidus-liquidus range

### 3.5 Pouring rates

As there was no system available in this series to measure the mass or volume flow entering the channel, this had to be calculated. After each experiment the spread masses of oxide and iron were weighed and compared to the calculated data. From these masses and the estimated densities of the iron and oxide melts ( $\rho_{\text{oxide}} = 2800 \text{ kg/m}^3$ ,  $\rho_{\text{iron}} = 6300 \text{ kg/m}^3$ ), the remaining volume of the melt and the melt level in the reaction crucible is calculated, at the point of time when the swamp volume is just filled up and spreading is about to start next.

For the flow out of a vessel under gravity, the relation between volume flow and liquid level is calculated with the Torricelli formula. Following equation gives the volumetric flow rate [10]:

$$\dot{V} = \mu \cdot A \cdot \sqrt{2 \cdot g \cdot H}$$

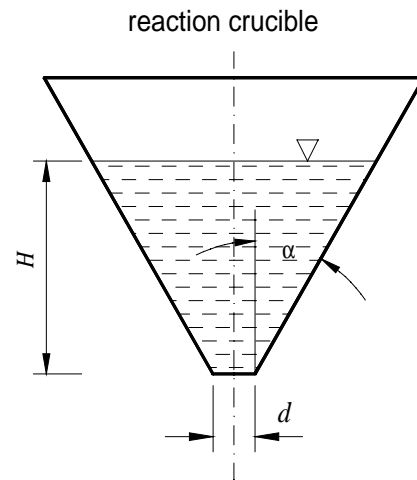
$\dot{V}$  = volumetric flow rate

$A$  = cross-sectional area of the nozzle

$H$  = melt level

$g$  = gravitational constant

$\mu$  = discharge coefficient



The pouring time in dependence on the melt level is given by [10]

$$t = \frac{1}{\mu \cdot A \cdot \sqrt{2 \cdot g}} \int_0^h \frac{A_H}{\sqrt{H}} \cdot dH$$

with  $A_H = f(H) = \frac{\pi}{4} (2 \cdot \tan \alpha \cdot H + d)^2$

$t$  = pouring duration

$A_H$  = cross-sectional area of the reaction crucible at melt level  $H$

Integration leads to

$$t = \frac{1}{\mu \cdot A \cdot \sqrt{2 \cdot g}} \cdot \left( \frac{2}{5} \pi \cdot (\tan \alpha)^2 \cdot H^{2.5} + \frac{2}{3} \pi \cdot (\tan \alpha) \cdot d \cdot H^{1.5} + \frac{1}{2} \pi \cdot d^2 \cdot H^{0.5} \right)$$

With the initial melt level (as described above), the melt outflow of each miniKATS test has been calculated. Figure 5 shows melt level and volume flow in dependence of the pouring time. The discharge coefficient [10] depends on the form of the nozzle and was set to 0.9 for these calculations. The pouring process lasts longest in miniKATS-3. A pouring duration of 7.2 s was calculated which corresponds to the observed time of ~7 s. For miniKATS-4 and -5 a pouring time of 6.3 s was calculated, a pouring time of ~6 s was observed in the video recordings. The calculated initial volume flow is 0.39 l/s for miniKATS-4 and -5. Complete data for all tests are given in Table 1.

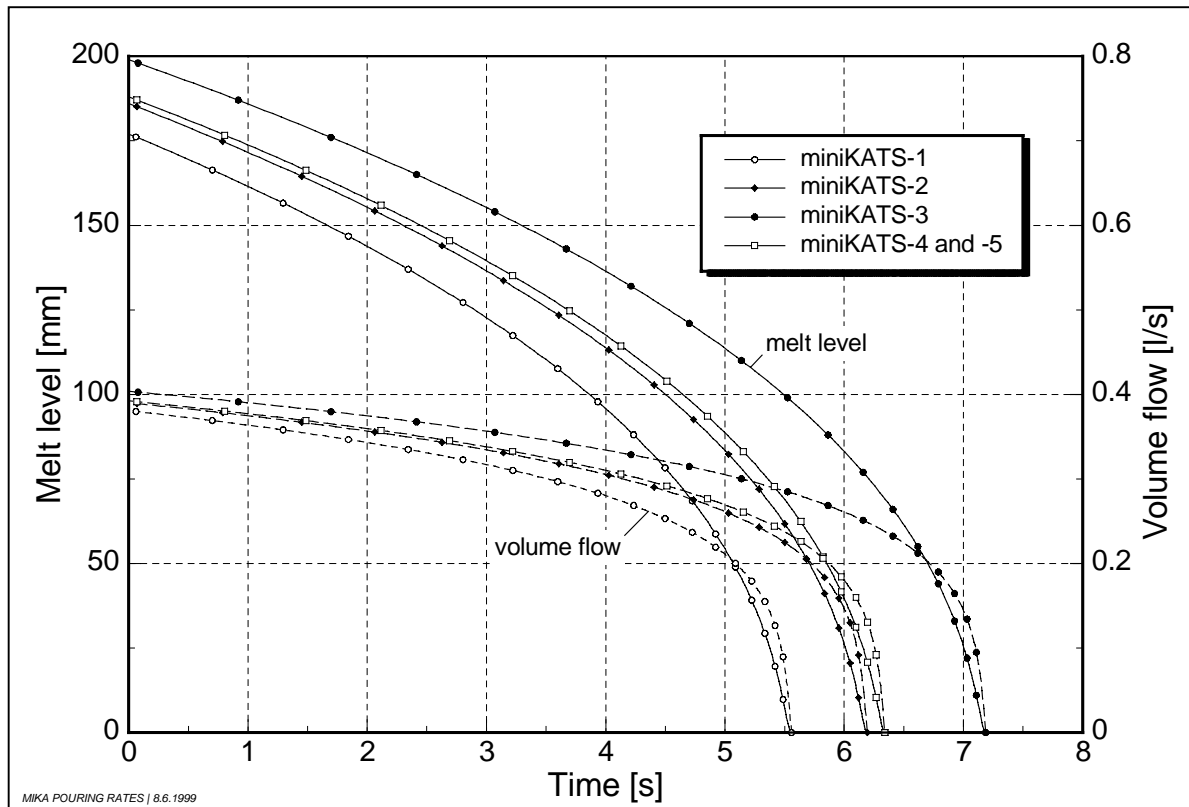


Figure 5: Calculated pouring rates and melt level of the finally spread melt in the miniKATS tests

## 4 Description of observed spreading behaviour

In the following each miniKATS experiment is described in detail. Experimental data like spread masses, pouring rate and duration, initial temperature, total spreading distance, etc, are given first (see also Table 1 and Table 2). Then the observations from the video and infrared video recordings are described and shown. A summary of the spreading characteristics is given in Table 3. Finally the results of post test analysis, appearance (colour, porosity, surface structure), thickness and shape of the cross-section of the solidified melt are discussed. The description is completed by a short summary where also first conclusions are drawn.

The spreading behaviour in miniKATS-1, where no quartz sand has been added to the thermite powder, was very different from the following experiments because the melt temperature was near (or even below) the liquidus temperature (Table 3).

In the other experiments the melt temperature was remarkably above the liquidus and the spreading was similar to that of a low viscosity liquid (like water), although

surface crusts have been observed in the later phase of spreading. There is no fundamental difference in spreading between miniKATS-2, -3, -4 and -5. This is not surprising, because although there is a difference in melt composition (miniKATS-2 without, the other three tests with addition of quartz sand) both  $T_{50\%}$  and  $T_{liq}$  are comparable in these tests.

In miniKATS-3 a rather large amount of iron spread together with the oxide melt and perhaps influenced the behaviour of the leading edge. However, the overall spreading does not appear to be different from the other tests.

From one test to the next one, the experimental setup was improved and finally in miniKATS-4 and -5 practically all iron was gathered in the swamp and pure oxide spreading was achieved. As the two tests are quite similar in initial temperature, spread mass and oxide composition, they can serve to judge the reproducibility of results.

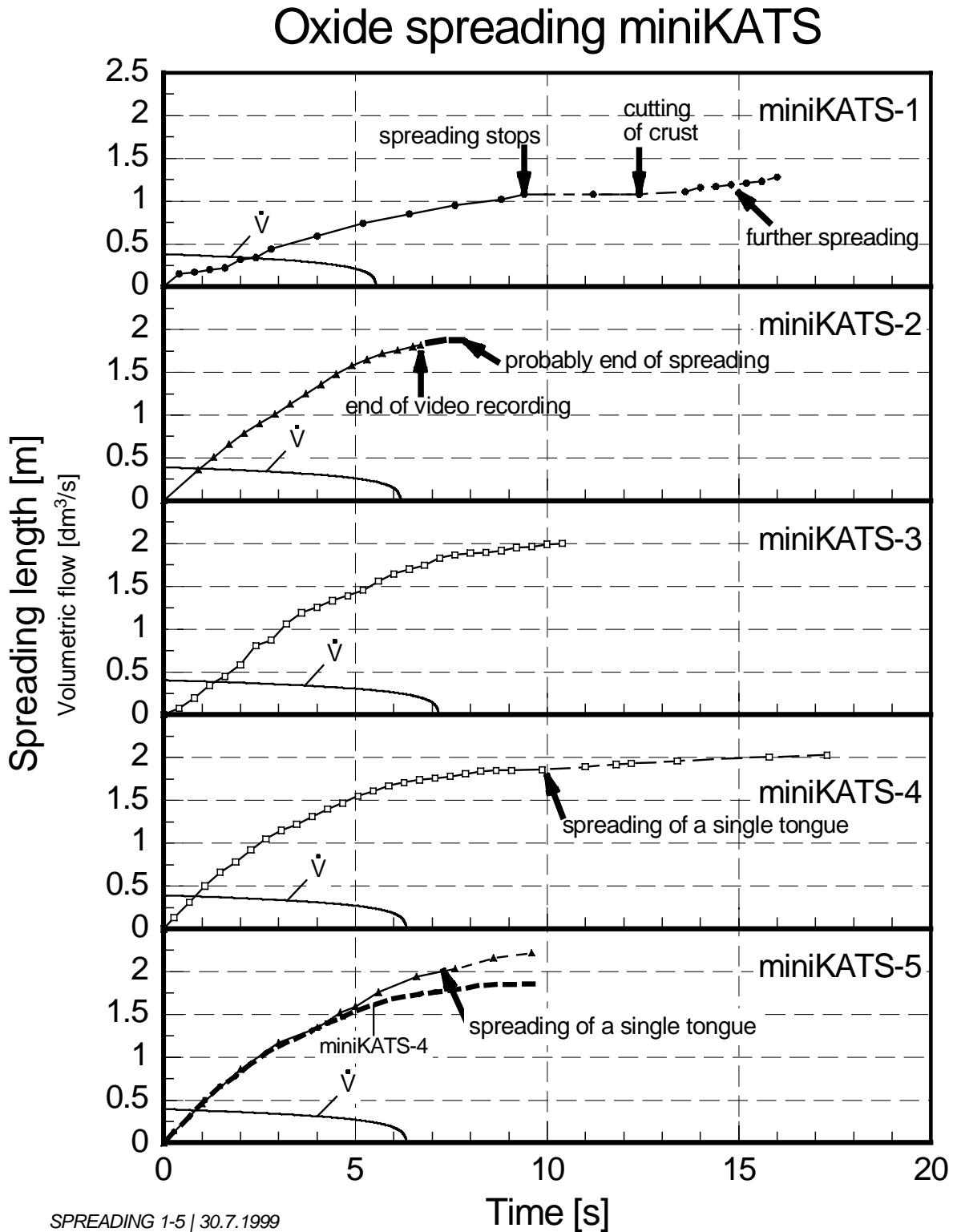


Figure 6: Transient spreading of oxide melt in miniKATS. Calculated volumetric flow rate is added.

## **4.1 *miniKATS-1***

After conduct of the experiment the spread melt was examined. Iron and oxide were separated and weighed. It was not always easy to separate iron and oxide because there was an intimate mixture over the whole length of the channel. The spread iron mass was roughly ~1 kg, the oxide mass ~4.32 kg. This large amount of iron that was not gathered in the swamp shows that the melt flow from the reaction crucible into the swamp and from there over the dam onto the channel was very turbulent and disturbed. The pouring duration could not be determined from the video recording. It was calculated to be 5.6 s with an initial volume flow rate of 0.38 l/s that decreases according to a polynomial root function (Figure 6).

The maximum of the temperature scale for the infrared video camera was set to 2036°C in this test. The maximum measured initial temperature of the spreading melt was 2015°C at 1.3 seconds after start of spreading: this means that the initial melt temperature was slightly below respectively near to the liquidus temperature  $T_{liq}$  (~2050°C, Table 3). This temperature was observed only in a small area, the neighbouring areas showed temperatures between 1990°C and 2000°C. The highest temperatures during the experiment are mainly observed close to the swamp outlet (15 cm behind the dam) and at the leading edge melt front. Near the outlet the temperature stays on this high level for about 7 s from start of spreading.

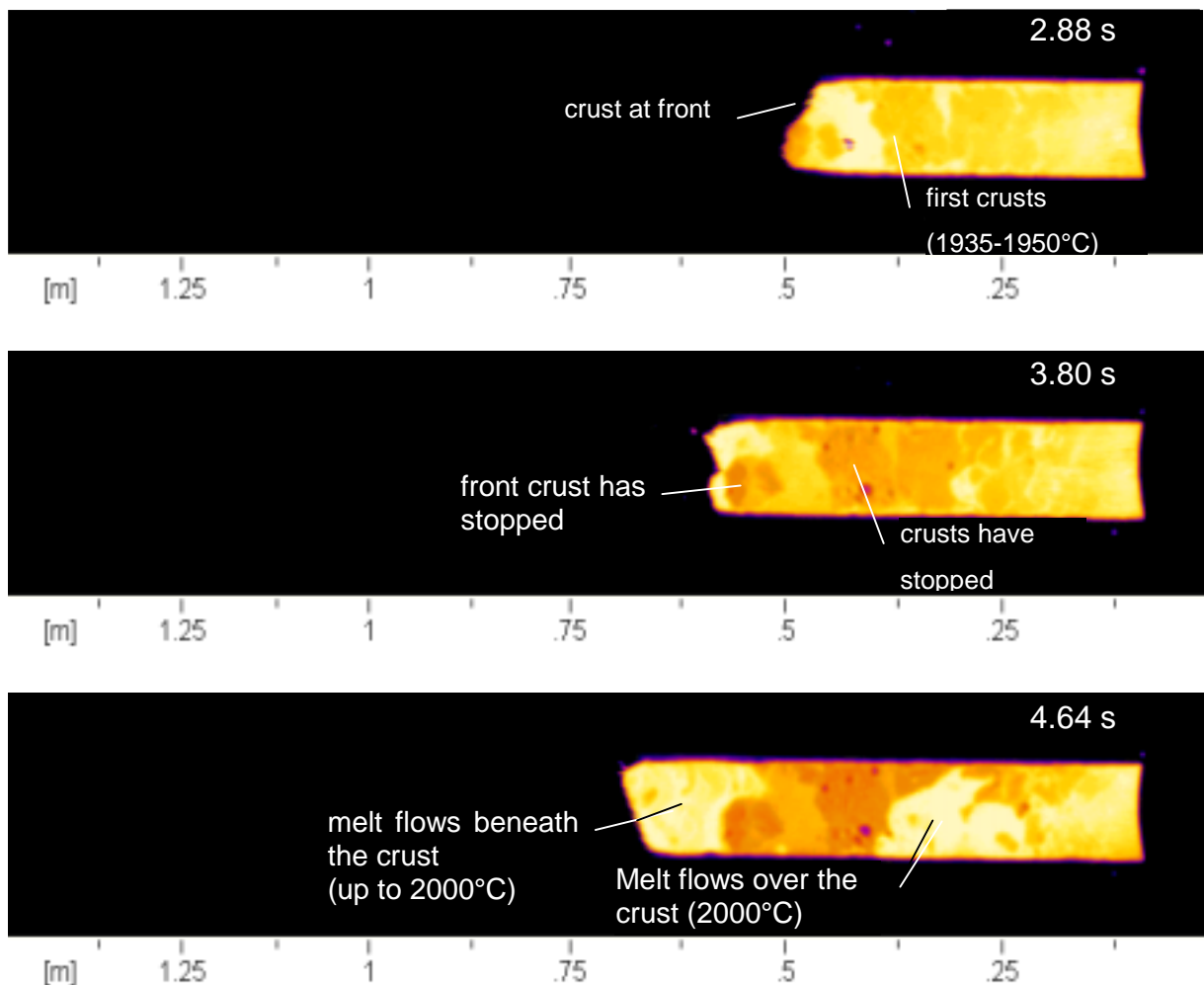
The transient spreading has been analysed with the help of the infrared video recording. Figure 6 shows the propagation of the leading edge of the spreading melt. Spreading starts 41.36 s after ignition, which is set to time zero in Figure 6 and also in the following discussion. The melt spreads over 1.08 m in 9.4 s and then stops suddenly. After 12.5 seconds the crust near the melt front was mechanically broken which leads to a further spreading of one single tongue of melt that stops at 1.28 m after 16 s.

### **4.1.1 Details of the spreading process (see Figure 6, Figure 7 and Table 3)**

The spreading on the first half-meter in the channel occurs intermittently. This behaviour could be caused by a discontinuous melt flow onto the channel because of turbulence in the swamp.

Quite early after start of spreading the formation of surface crusts can be observed. Already at 2.9 seconds, a rather large area of the spreading melt, about 10 cm be-

hind the propagating melt front, is covered by crusts. They are easily identified because of their shape, which does not change during transport, also by the low temperature ( $T_{\text{crust}} 1935^{\circ}\text{C} - 1950^{\circ}\text{C}$ ) in comparison to the temperature of the surrounding ( $1990^{\circ}\text{C} - 2000^{\circ}\text{C}$ ). It seems reasonable that the observed crust temperature  $T_{\text{crust}}$  is near to the calculated  $T_{50\%}$  ( $\sim 1950^{\circ}\text{C}$ , Table 3). These crusts float downstream with the melt at the same velocity as the melt front, until they are caught and anchored by freezing at the channel walls at 3.8 s. At this time, the surface temperature of the crust cooled down to  $1870^{\circ}\text{C} - 1890^{\circ}\text{C}$ . The front propagation is not influenced by the stop of the crusts, fresh melt flow emerges from underneath these crusts and continues spreading, and the front propagation is fed by this flow. At the same time the anchored crusts are also top flooded by hot melt ( $\sim 2005^{\circ}\text{C}$ ).



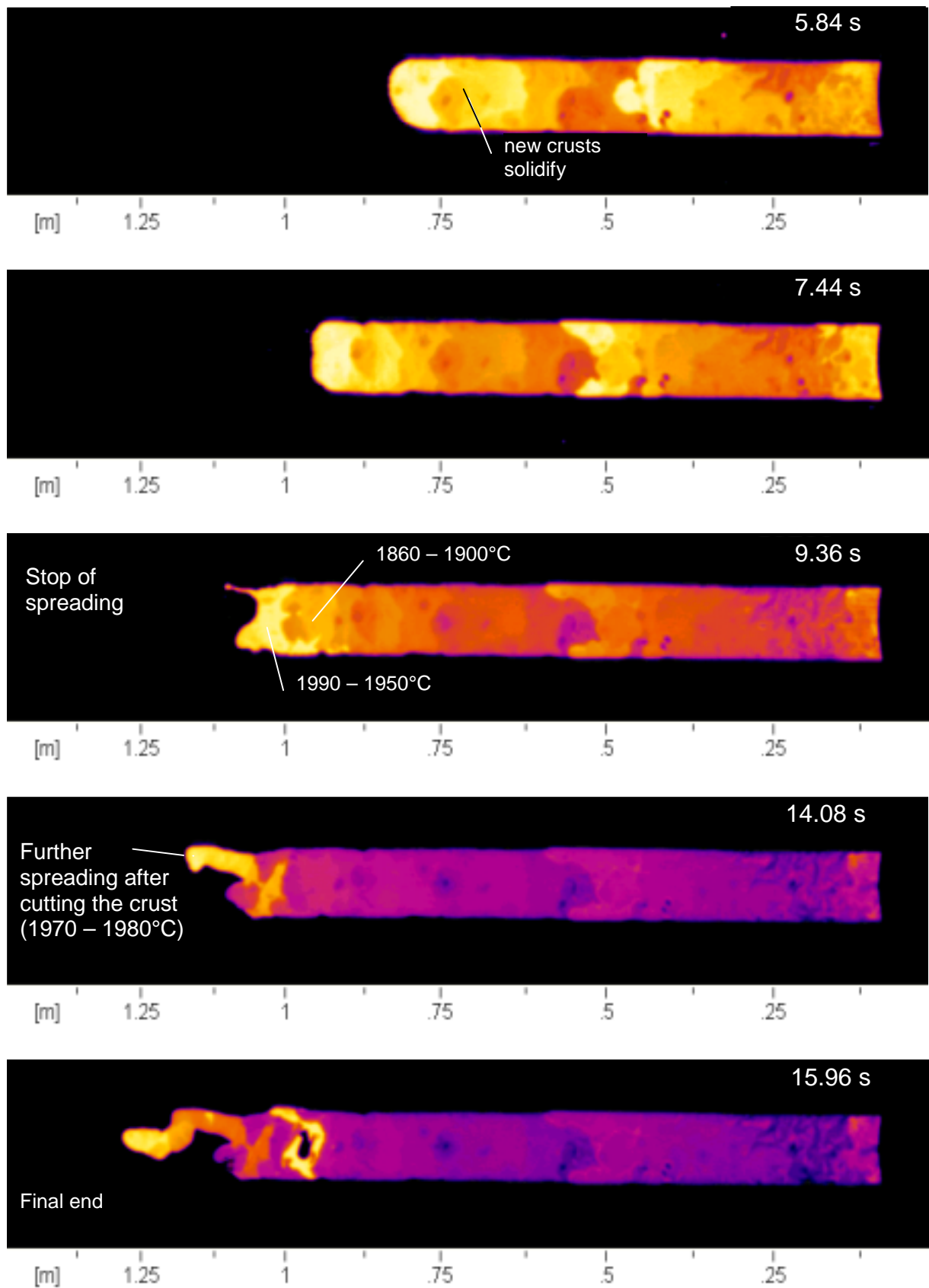


Figure 7: Melt surface infrared pictures in miniKATS-1 at different times

At 3.7 s a crust floating at the melt front and covering half of the channel width stops and hot melt emerges from underneath without a significant change in melt front velocity (these are only two phenomena typical for a lot of similar processes observed during the spreading).

The melt front changes its shape continuously till the end of spreading. This demonstrates that the leading edge is never completely covered by surface crusts. Temperatures at the front stay very high. When the spreading stops after 9.4 s (at 1.08 m) the temperature at the melt front is still between 1950°C and 1990°C which is above  $T_{\text{crust}}$  (<1950°C). At this time the region < 1m is covered by a crust having surface temperatures between 1860°C and 1900°C, these temperatures are decreasing steadily towards the melt outlet. So it seems that at the moment of immobilization the leading edge was not covered by a crust and therefore stopping was not caused by crust formation. One reason for this could be that the driving gravitational pressure dropped beneath the surface tension pressure. The pressures are balancing each other at a melt height of 9.3 mm (calculated for a pure alumina melt, see above). It is not easy to determine the melt height at the leading edge in the moment of the first stop because the front structure was mechanically destroyed after melt stop and the surface is therefore very uneven and rutted afterwards. Some pieces of solidified melt from the corresponding region were examined after the experiment and their height is about 10 to 11 mm. This could be an indication that the surface tension caused stop of spreading.

12.5 s after start and 3.1 s after end of spreading the surface temperature at the front has cooled down to 1800°C – 1820°C. At this time the front structure was mechanically broken up to investigate the bulk area of the melt. This breaking-up lead to a further spreading of one single tongue (~100 cm<sup>3</sup>) of oxide melt with a temperature 1970°C – 1980°C. This tongue solidified with a height of 9 – 10 mm which is again in good agreement with the calculated melt height at gravitation / surface tension equilibrium.

A few seconds later, the crust between 1 m and 70 cm was broken mechanically several times with the hatchet and after each hit hot melt becomes visible again. But most of the melt that was released from these gaps was iron which has a low solidification temperature of 1560°C.

#### **4.1.2 Post-test examination**

In comparison to all other miniKATS tests, the surface of the spread melt in miniKATS-1 was the most uneven one. The surface is gathered in folds where crusts have been moved against each other. It is still visible where hot melt has flown over crusts because the melt is several millimetres higher there and forms a small but clearly visible step (at 50 cm in the channel).

The melt did not completely occupy the whole channel cross-section (bad wetting). From 0.5 m towards the end of spreading the melt solidifies in a convex cross-section that sometimes leaves a gap of a few millimetres between the crust and the channel walls (probably due to thermal shrinkage of the frozen melt). The melt level is higher in the middle of the channel and lower at the walls.

The solidified melt between melt outlet and 0.9 m is between 15 and 25 mm high and very uneven. It is interspersed with systems of cavities. At the first stop of spreading the melt height was ~11 mm, the height of the single tongue was only 9 - 10 mm.

The solidified melt has a dark grey colour.

#### **4.1.3 Summary**

Whereas in all other tests with superheated melts, in miniKATS-1 the initial melt temperature was near and probably slightly below  $T_{liq}$ , causing early and massive crust formation. Although crust formation did not principally hinder spreading because melt flow proceeded beneath and/or over the crusts without deceleration of the front velocity, it causes immobilization of a large part of melt, leading to a pretty high thickness of the slug (15 – 20 mm) near the melt outlet. The first stop of the melt spreading is probably due to surface tension balancing the gravitational pressure. In the moment of immobilization, the melt front is not covered by crusts. The further spreading of a small amount of melt, after the crust at the melt front has been broken, shows, that under the crusts there is still melt present at nearly initial temperature (no bulk freezing, no increase of bulk viscosity). Solidification processes are surface dominated.

## 4.2 *miniKATS-2*

The amounts of iron and oxide masses have been weighed separately after the experiment. As in miniKATS-1 not all the iron was gathered in the swamp. The iron mass in the spreading channel was 0.58 kg and the oxide mass 5.14 kg. It was not possible to determine the pouring duration from the video recording. It was calculated to be 6.2 s with an initial volume flow of 0.39 l/s that declines according to a polynomial root function, (see Figure 6).

The maximum of the temperature scale for the infrared camera was set to 2128°C and this temperature was recorded over a large area up to 40 cm from melt inlet. Within this area the surface temperature stays partially on this level for about 5 s after start of spreading. It seems that the initial temperature was much higher than the maximum scale value. Towards the propagating melt front the temperature decreases. According to the calculated liquidus temperature  $T_{\text{liq}}$  (~1850°C, Table 3), the melt was strongly superheated (>280°C). But, in contrary to miniKATS-1, where the calculated  $T_{50\%}$  and observed  $T_{\text{crust}}$  go quite well together, there is a discrepancy of these two temperatures for miniKATS-2. A liquidus temperature of  $T_{\text{liq}} \leq 1850^\circ\text{C}$  was calculated with the GEMINI code for the miniKATS-2 oxide composition. The experimentally observed temperature of crust formation ( $T_{\text{crust}}$ ), however, was 1880°C – 1900°C (see below). This causes some doubts concerning the accuracy and reliability of the characteristic temperatures measured and/or calculated with GEMINI. Nevertheless, the oxide melt of miniKATS-2 was strongly superheated with a temperature range of >230°C between initial temperature and temperature of crust formation. The transient spreading has been analysed with the help of the infrared and normal video recordings. Figure 6 shows the propagation of the leading edge of the spreading melt. Spreading starts about 20 s after ignition. The melt spreads very quickly in a continuous and uniform flow and stops after 7.5 s at a distance of >1.83 m. After 9 seconds the front structure is mechanically broken up which leads to a further spreading.

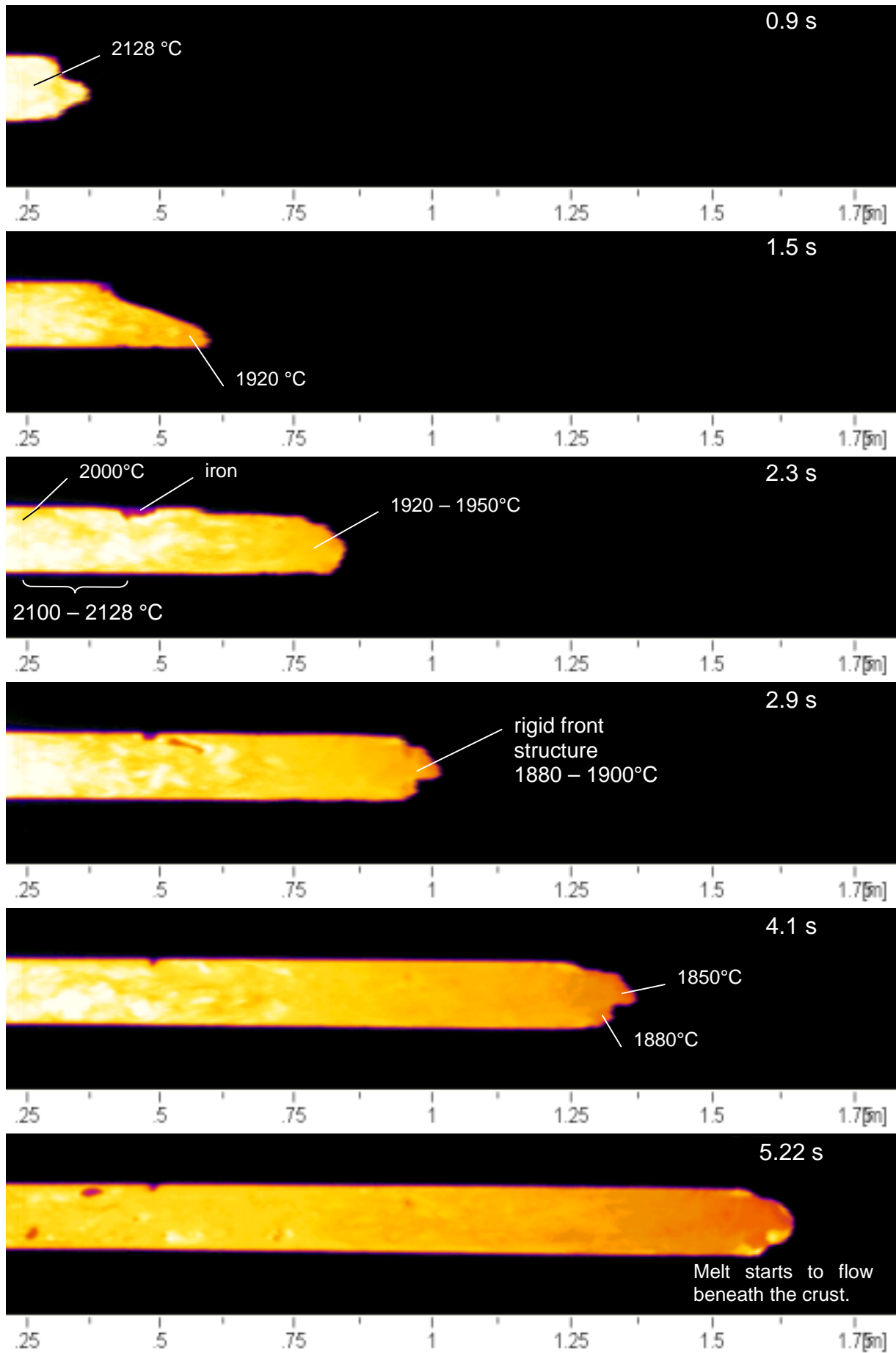
#### 4.2.1 Details of the spreading process (Figure 6 and Figure 8)

The following observations are from the infrared video recording, Figure 8. Unfortunately the visible range of the channel for the infrared camera is only from 0.2 m to 1.83 m, so the exact point of time of the beginning of spreading cannot directly be determined. If the graph of front propagation versus time is extrapolated back to the start of the channel at the dam the moment of start of spreading is determined to 19.5 s after ignition. This time corresponds to zero in Figure 6.

For the first two seconds of spreading, the melt front is very uneven across the channel width. The maximum difference in spreading lengths between the right and the left channel wall is 15 cm. The data of melt propagation in Figure 6 correspond to the very front of the melt.

Up to 2.3 s after start of spreading, corresponding to about 0.8 m in spreading distance, the melt front changes its shape continuously, which is an indication that no stable crusts have been formed there yet. But at 2.9 s (~1 m spreading distance), the shape of the front seems to be frozen, yet no change in the spreading velocity is observed. The melt surface temperature at the leading edge is between 1880°C and 1900°C, only a few centimetres behind the leading edge amounts to 1920°C. At the same time the melt temperature 20 cm from melt outlet is still  $\geq 2128^\circ\text{C}$ .

This solidified front crust is floating and transported by the melt flow until it stops 5.6 s after start of spreading at a distance of ~1.67 m: the crust decelerates and at the same time hot melt flows underneath the crust emerges and continues spreading without a significant change in velocity. For a short time, a maximum melt temperature of 2050-2080°C is observed for this “new” emerging melt, but it quickly cools down to  $<2000^\circ\text{C}$ . Together with the stop of the front crust at 5.6 s the movement of the whole melt surface crust, except that of the new front, stops. Up to this moment there has always been some kind of movement of the melt surface, either of smaller crusts or just of streaks.



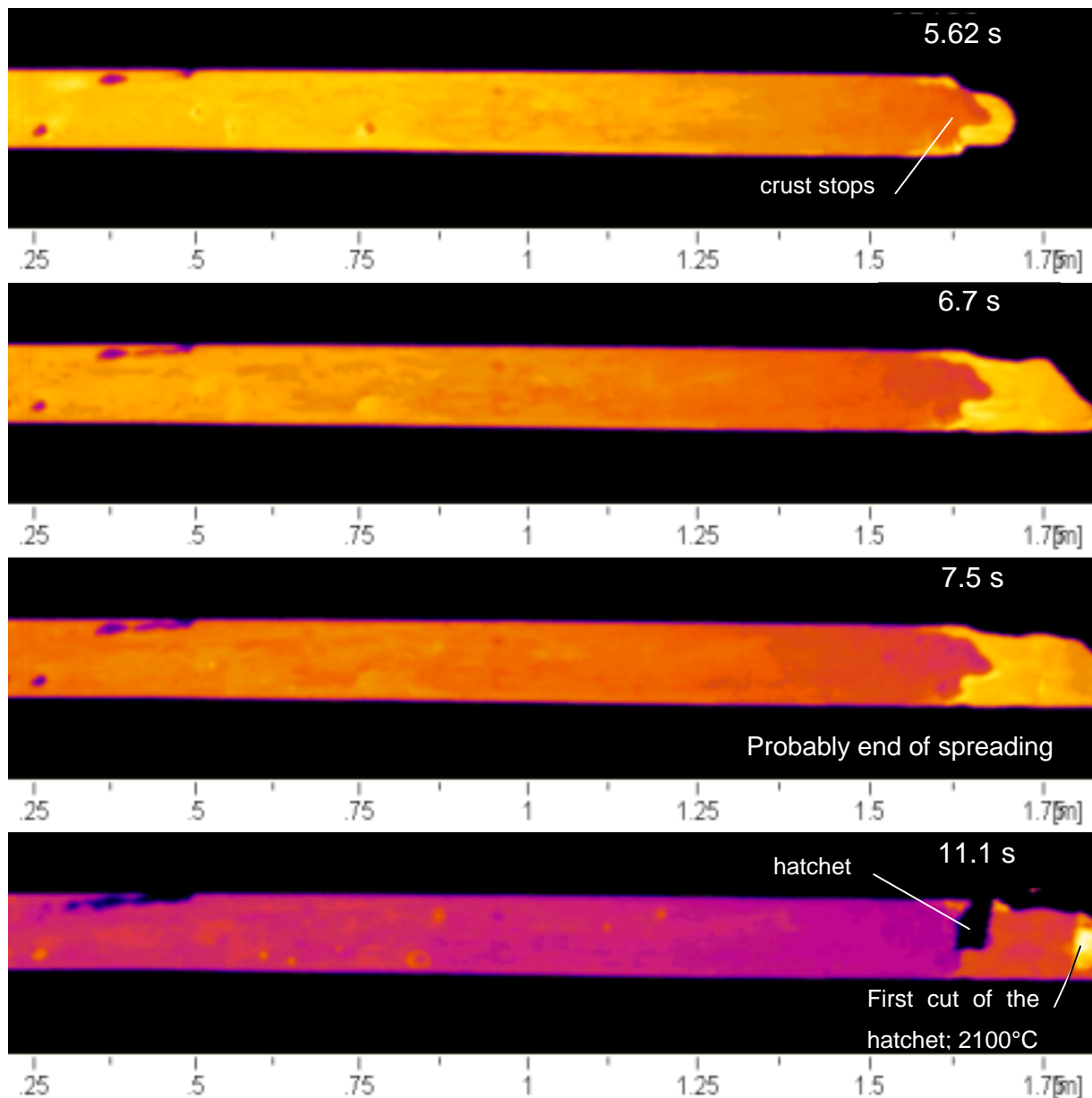


Figure 8: Melt surface infrared pictures in miniKATS-2 at different times

Compared to miniKATS-1, the melt temperature was more than 100 K higher and the melt was strongly superheated. Correspondingly, the spreading of miniKATS-2 is faster and over longer distances and the spreading process is not so much influenced by early crust formation. Unfortunately, the stop of spreading was just outside the range of view of both the video and the infrared camera. The melt reaches the 1.83 m range of the video at 6.7 s. The total spreading length is known from the mark it left on the spreading channel. The very edge of the sloping melt front reached a distance of 1.86 m, which is close to the range limit of the infrared camera (1.83 m). 9 s after the beginning of spreading the front part of the crust was cut by the hatchet, the location is still within the range of the infrared camera. Immediately a melt tem-

perature of 2100°C was measured by the infrared system at the cut. The overview video shows further spreading of the melt. At 12.3 s once more the hatchet cut the crust at 1.63 m and all the material which was located further downstream in the channel wiped off from the channel by the movement of the hatchet. At the open channel end the material falls down to the floor. The overview video shows both crusts falling and hot melt dripping on the ground. After the test many small pieces of hollow crust were found (enclosed liquid melt drained out and left a solidified surface crust).

#### **4.2.2 Post-test examination**

The solidified melt looks much different than that of miniKATS-1. The surface is very smooth. The melt occupied the channel cross-section completely. The thickness of the frozen melt is much smaller than in miniKATS-1, e.g. at 0.5 m the melt height in the middle of the channel was only 7 mm and 10 – 11 mm at the walls (concave shape, good wetting). The cross-sections of the bottom and top crusts show dendritic growth of crystals from the bottom and from the top towards the center with a sharp borderline in the middle, Figure 9. The concave shaped cross-section turns into a convex one towards the end of spreading. One piece taken from 1.4 m position shows melt heights of 9 – 10 mm in the middle of the channel and a convex curvature near the wall. From about 1.4 m towards the end of spreading, hollow pieces of crust are found, where the liquid melt has run out and left behind the solidified surface and bottom crusts which are connected together at the channel wall. One piece for example has an upper crust thickness of 1.4 mm and a bottom crust of 1.7 – 2.3 mm with a total height of 10 mm. The inner surface of this hollow is very smooth. The colour of the melt surface is a light brown. The cross-section shows a brighter colour with a touch of red.



Figure 9: Cross-section of the solidified melt after the test

#### 4.2.3 Summary

In this miniKATS-test there is a very quick, continuous and smooth spreading. This is different to miniKATS-1. Solidification does not start as early as in miniKATS-1, because the melt initial temperature is higher and solidification temperature seems to be a bit lower ( $<1900^{\circ}\text{C}$ ). Solidification starts at the leading edge and extends backwards against the spreading direction. Crust formation did not hinder spreading because melt flow continued beneath the crust, and had only a slight influence on the overall spreading. This is indicated by the fact, that the slug thickness is essentially constant over the spreading distance and equal to  $h_{\min}$  (equilibrium of gravitational and surface tension pressure). The first stop of the melt spreading is probably due to surface tension balancing the gravitational pressure. The further spreading with initial melt temperature after cutting of the crust shows that there is no bulk freezing. Liquid spreads further and leaves hollow crusts.

### 4.3 *miniKATS-3*

The separation of iron and oxide melts in test *miniKATS-3* did not work satisfactory, here the largest amount of iron was found on the spreading channel. After the experiment iron and oxide were separated from each other as well as possible and weighed. The iron mass in the spreading channel is ~1.8 kg and the oxide mass is ~5.7 kg. From the video recording a pouring duration of about 7 s was determined. The calculated value is 7.2 s with an initial volume flow of 0.40 l/s that declines according to a polynomial root function (Figure 6).

The maximum of the temperature scale was again 2128°C and this value was observed for some smaller areas near the melt outlet but only for short periods of time. It seems that the infrared measurement was slightly disturbed by smoke. Nevertheless, the temperature seems to be lower than in *miniKATS-2* where larger areas with temperatures of 2128°C and above were observed. The temperature near the melt outlet stays above 2030°C for at least 6.5 s after start of spreading. From the melt outlet towards the propagating melt front the temperature decreases steadily. There are no hot areas at the melt front as was observed in *miniKATS-1*. According to the calculated  $T_{liq}$  (~1900°C, Table 3) the melt was again strongly superheated (~250°C). The transient spreading has been analysed with the help of the infrared and normal video recording. Figure 6 shows the propagation of the leading edge of the spreading melt. Here the spreading length is averaged over the channel width. Spreading starts 29.72 s after ignition. The melt spreads with nearly the same velocity as in *miniKATS-2* and one tongue (iron) stops after 10.4 s at a distance of 2.0 m and the other tongue (oxide) stops after 13.4 s, 3 cm behind the first tongue. When the oxide tongue was finally hit by the hatchet, 19 s after start of spreading, no further spreading occurs.

#### 4.3.1 Details of the spreading process

The experiment *miniKATS-3* cannot be analysed with regard to temperatures at the leading edge, temperatures of earliest surface crusts and melt front structure, because of the high amount of iron that was found on the spreading surface, especially right at the leading edge. That surely has influence on the spreading behaviour, though the front propagation according to Figure 6 does not show any abnormalities.

Nevertheless, some qualitative observations should be shortly mentioned here. One interesting observation was made, possible by an improvement of the use of filters for the video recording, which made it easier to observe the surface structures during the spreading process. It is clearly visible that the bulk melt spreading is superposed by some sort of surface waves which travelled in spreading direction but with higher velocity than the propagation velocity of the leading edge, so that from time to time the leading edge is overtaken by these waves. It can further be seen how the melt surface solidifies. Solidification starts at the melt front, but this has no influence on the spreading velocity, and extends backwards towards the melt inlet. The surface waves mentioned above die out during this growing solidification process. At the same time the solidification proceeds from the channel walls towards the axis of the channel. The combination of these two freezing processes leads to a V-shaped freezing borderline that moves opposite to the spreading direction.

#### **4.3.2 Post-test examination**

The solidified melt looks much like the melt of miniKATS-2, though in miniKATS-3 quartz sand was added to the thermite. The surface is very smooth, the colour brown or grey. The cross-section shows a brighter colour with a touch of red. The concave shape of the cross-section turns into a convex shape towards the end of spreading. The concave shape shows that the melt level during spreading was higher than found after the experiment. When the solidification started first at the channel walls, the melt level stayed high there and dropped in the middle of the channel. Some interesting pieces prove this: the cross-sections show an upper and a lower layer of the same thickness and it looks as if the layers have collapsed after flow out of the hot liquid melt that was in between. The heights of the oxide crusts at the sidewalls are between 10 and 14 mm and 7 – 8 mm in the middle of the channel. From 1.75 m to 2 m, a thickness of 8 – 9.5 mm was measured. This is again an indication that stop of spreading is determined by the balance between gravitational and surface tension pressure.

## 4.4 *miniKATS-4*

Due to improvements in the separation of iron and oxide, only 0.1 kg of iron was found on the first 10 cm of the spreading channel. The oxide mass was 5.44 kg. From video recording a pouring duration of about 6 s was determined. The calculated value is 6.3 s with an initial volume flow of 0.39 l/s that declines according to a polynomial root function (Figure 6).

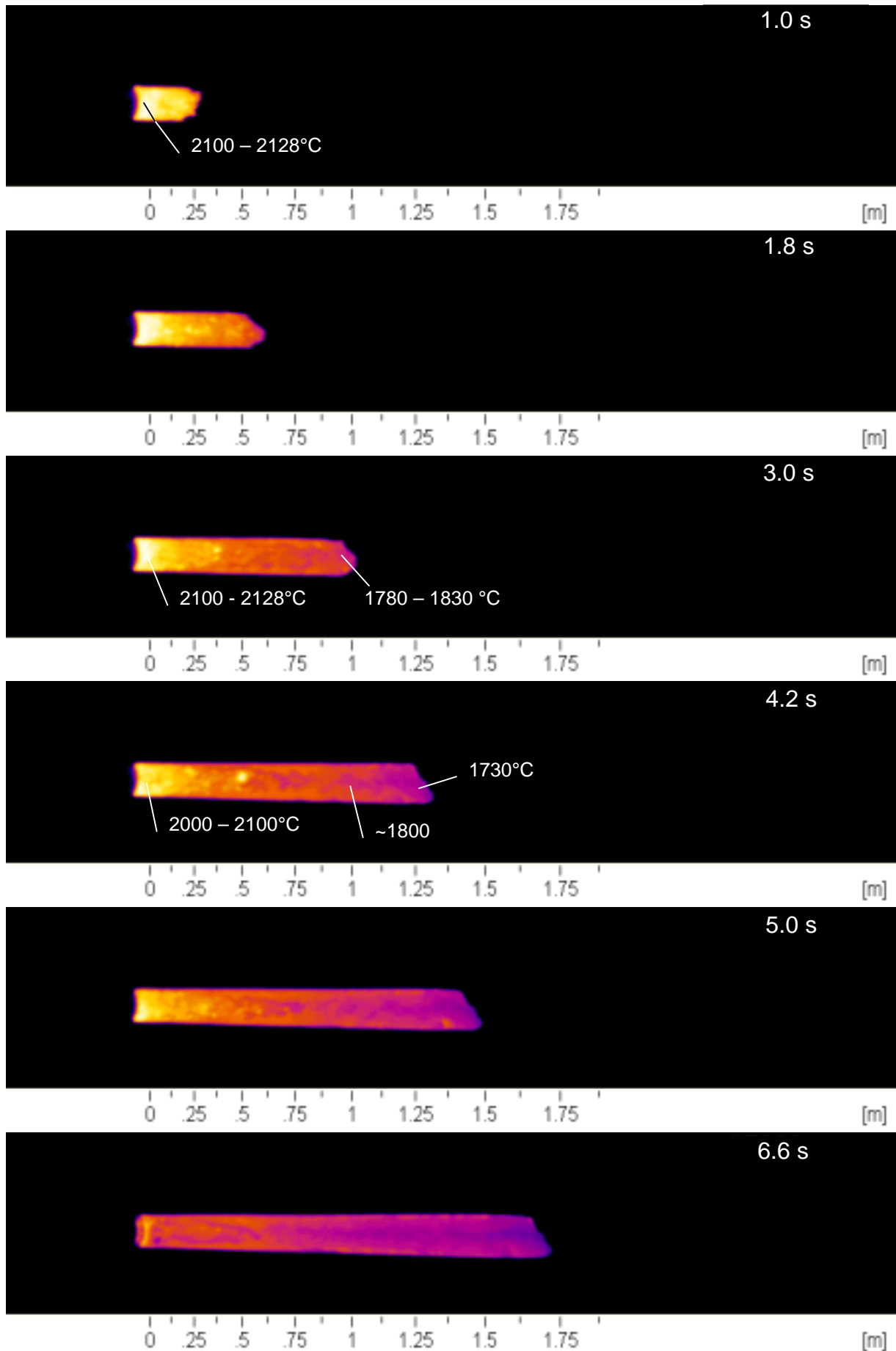
The maximum of the temperature scale was again 2128°C and this value was reached at some areas near the melt outlet. The melt outlet temperature stays above 2030°C for at least 5 s from start of spreading. From the melt outlet towards the propagating melt front the temperature decreases. There are no hot areas detected at the melt front. According to the calculated liquidus temperature  $T_{\text{liq}} \sim 1900^\circ\text{C}$  and to the observed crust temperature  $T_{\text{crust}}$  (1780°C – 1800°C; see below) the melt was strongly superheated. Again, as in miniKATS-2, there is a discrepancy between the experimentally observed  $T_{\text{crust}}$  and the calculated  $T_{50\%}$  ( $\sim 1670^\circ\text{C}$ ; Table 3).

The transient spreading has been analysed with the help of the infrared and video recordings. Figure 6 shows the propagation of the leading edge of the spreading melt, it is averaged over the channel width. Spreading starts 30.72 s after ignition and is quite homogeneously over the channel width for a period of 9.5 s (1.85 m). Then only a small tongue of about one third of the channel width continues on to spread very slowly. When the hatchet hits the end of this tongue 15.9 s after start of spreading, no further spreading occurs.

### 4.4.1 Details of the spreading process (Figure 6 and Figure 10)

As mentioned above, the spreading behaviour in the tests miniKATS-2, -3, -4 and -5 is very similar. With the video recordings of miniKATS-4 it can again be observed, that solidification starts at the leading edge and extends back towards the melt outlet, Figure 10. Thus, on a large area, a constantly growing surface crust builds up which moves as a whole during spreading. Also the travelling of surface waves can be observed from the video recording.

Description of observed spreading behaviour



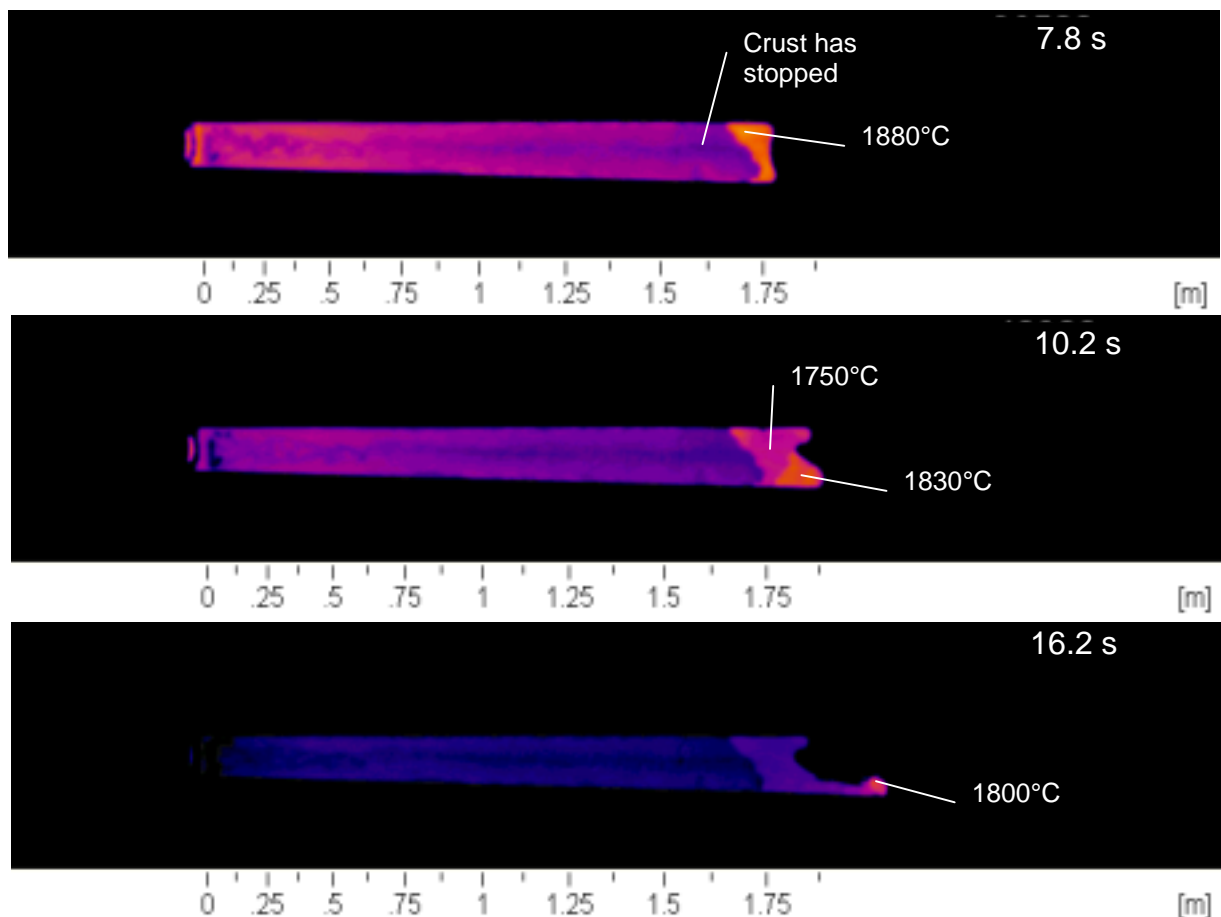


Figure 10: Melt surface infrared pictures in miniKATS-4 at different times

About 4 s after start of spreading, the melt 20 cm behind the melt front is characterised by its calm surface, it seems that this is the beginning of solidification. At this time the temperature at the leading edge is between 1780°C and 1800°C. Back in the mentioned “20 cm”-area the temperature is between 1800°C and 1830°C, which is in between the calculated  $T_{liq}$  and  $T_{50\%}$  (Table 3).

After 4 s, the leading edge does not change its shape anymore. This is an indication for a solid crust that floats on top of the hot liquid melt. Temperatures of the crust are between 1700°C and 1730°C. The movement of the crust stops 6.9 s after start of spreading at a distance of 1.75 m and at the same time further spreading of hot melt emerging from beneath the crust continues with a temperature of 1900°C. In this experiment a photo camera with motor winder (up to 4 pictures per second) was used for the first time and took some pictures of this event. These pictures show that the surface crust, which appears much darker than the hot melt, is lifted a bit as the hot melt finds its way beneath the crust. Similar pictures are shown in the section of miniKATS-5 where the same phenomena were observed.

The spreading then continues quite homogeneously over the channel width up to a distance of 1.85 m (9.5 s after start of spreading). From there on, only a small melt tongue of about one third of the channel width continues spreading very slowly. At the time when the hatchet hits the end of this tongue after 15.9 s, the spreading did not have come to an end yet. Because of the small height of this tongue of only 9 mm there was only a small amount of melt available inside this tongue, therefore no further spreading occurs. A second strike with the hatchet after 17,3 s leaves the melt tongue with a final spreading length of 2.03 m and a surface temperature of 1830°C maximum.

#### **4.4.2 Post-test examination**

The colour of the melt (dark grey) is somewhat different from miniKATS-2 and –3 (brown, grey). The crust surface is again very smooth. Along the axis of the channel, especially between 0 m and 1.5 m, some sort of vortex structure is visible. From 0.6 m back to the melt outlet a V-shaped area is clearly visible by its different crystal structure: The crystals are much larger than in the other parts of the melt surface. As mentioned above, solidification extends from the melt front back towards the melt outlet and from the sidewalls towards middle of the channel. So the special crystal structure is probably due to the fact that this area was the last one to cool down and therefore the temperature dropped more slowly which led to larger crystal formation. The crust thickness at the front is about 9 mm. Up to 1.5 m it is higher near the walls (9-11 mm) and lower in the middle of the channel (7 – 8 mm). The final melt height is close to the minimum value,  $h \sim h_{\min}$ , near the melt front, and again indicates that immobilisation of the spreading melt is caused by the balance of gravitational and surface tension pressure.

#### **4.4.3 Summary**

The spreading is very quick, continuous and smooth similar as in miniKATS-2 and –3. Crust formation did not hinder spreading because melt flow continued from beneath the crust, and had essentially no influence on overall spreading, as indicated by the constant crust thickness equal to  $h_{\min}$ . Determination of  $T_{\text{crust}}$  is more difficult than in miniKATS-1 or –2. The transition from a high viscous melt surface to a more and more rigid crust seems to start at temperatures between 1780°C to 1800°C and

is finished between 1730°C and 1700°C. This extended solidification range is probably due to the addition of SiO<sub>2</sub>. Spreading in miniKATS-2 and -4 (Figure 6) is quite similar up to 7.5 s, but whereas in miniKATS-2 spreading stopped at this time, in miniKATS-4 it continues very slowly as a single creeping tongue.

#### **4.5 miniKATS-5**

The separation of iron and oxide melts worked again very well, no iron was found on the spreading channel. The oxide mass was 5.62 kg. From video recording a pouring duration of about 5.9 s was determined. The calculated value is 6.3 s with an initial volume flow of 0.39 l/s that declines according to a polynomial root function (Figure 6).

The maximum of the temperature scale was again 2128°C and this temperature was observed at some areas near the melt outlet. As the infrared camera was positioned on a lower level to observe the melt front in more detail, temperature measurement at specified channel positions are not accurate. Again the melt was strongly superheated (~250°C).

The transient spreading has been analysed with the help of the normal video recording. Figure 6 shows the propagation of the leading edge (averaged over the channel width) of the spreading melt. Spreading starts 32.96 s after ignition and continues over the whole channel width for a period of 7.2 s reaching a length of 2.0 m. From then on only half of the channel width is covered by a single tongue, that continues spreading until 9.6 s after start and reaches 2.22 m in the channel. When the hatchet hits the end of this tongue 12 s after start of spreading, no further spreading occurs.

##### **4.5.1 Details of the spreading process (Figure 6, Figure 11 to Figure 15)**

Spreading starts 32.96 s after ignition. For the first 5 s, the graphs of miniKATS-4 and -5 in Figure 6 are almost congruent. But whereas spreading of miniKATS-4 decelerates in the following, the melt of miniKATS-5 keeps up the speed for a longer time and reaches a spreading length of 2 m after 7.2 s.

For times later than 5 s, the leading edge does not change its shape anymore, which is an indication that a crust has formed that is rigid enough to float as a whole on top of the liquid melt underneath. On both infrared video (Figure 11) and photos (Figure 12 to Figure 14) it is visible that the crust floats on a cushion of hot melt. The crust

covers nearly the whole curvature of the leading edge, but at some spots, especially on the left side of the channel, the hot underground is visible. The photo camera started 3.24 s after start of spreading, taking a picture every 0.22 s, which is nearly 4.5 pictures per second.

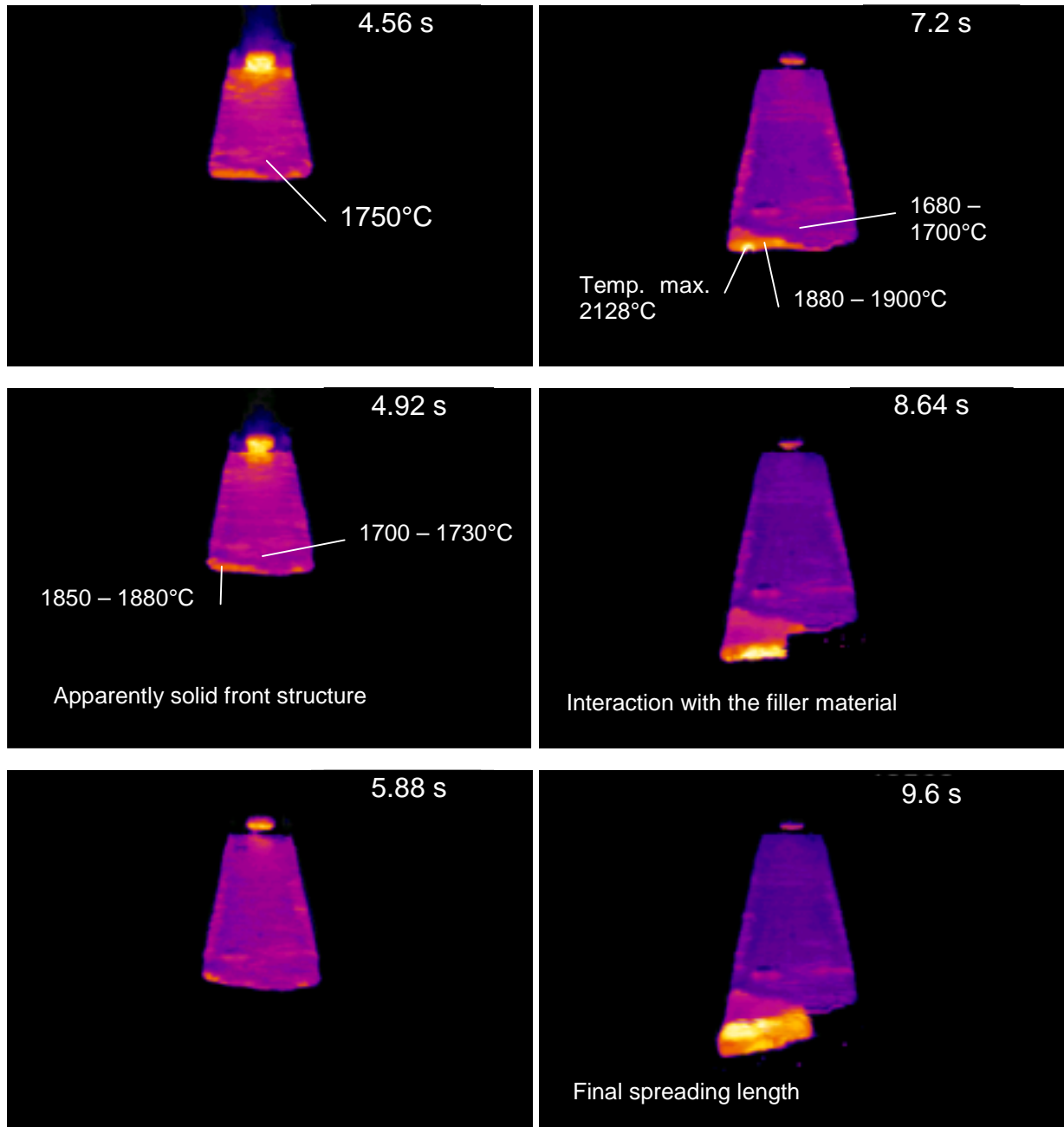


Figure 11: Melt surface infrared pictures in miniKATS-5 at different times

The first couple of pictures were out of focus range, the depth of focal length was set to the anticipated range of maximum spreading. One early picture (Figure 11 and Figure 12), taken 4.6 s and 5.9 s after start of spreading, shows a melt surface

structure that looks as if locally a thin skin has been formed. Only a few pictures later an apparently solid crust has been already formed, as observed from infrared video. The temperature of the “skin” is about 1750°C (Figure 11). As mentioned above, in miniKATS-5 the temperature measurement is not so accurate due to the unfavourable perspective of the infrared camera. The hot spot on the left side of the leading edge shows temperatures of 1850 - 1880°C. The floating of the surface crust stops after 7.2 s. The surface temperature of the crust at this time is decreased to 1680°C – 1700°C. The crust is lifted at the front, when the hot melt underneath starts to continue spreading further on. But only on the left side of the channel (where the hot spot was detected earlier) the spreading continues for another 0.22 m. The surface temperature of this new tongue of melt is between 1880°C and 1900°C. A small piece of metal that inadvertently lay on the spreading channel gets flown over by the melt, thereby disturbing the melt surface and giving sight for a short moment to the bulk of the melt with a temperature that still topped the temperature scale (2128°C). This shows that the bulk temperature is much higher than the surface temperature. Both video and photos show that the shape of the leading edge is rounded. This proves that surface tension plays a role in the final spreading of these oxide melts. After 8.6 s the tongue on the left side reaches a part of the spreading channel that was repaired with a filler based on organic/ceramic material to cover a hole that was left by a former miniKATS test. The spreading was not expected to reach that far. The water content of this filler material interacted with the hot melt and the emanating water vapour stirred the melt. This event stopped the spreading of the melt essentially. The final spreading length is 2.22 m, which was reached 9.6 s after start of spreading. The melt-water interaction lasts till 12 s, as the hatchet hits the leading edge. But this does not lead to further spreading. Due to the vapour induced melt bubbling, bulk temperatures could be observed (<2000°C). Whereas in miniKATS-4 the single tongue spread very slowly for a quite long time in miniKATS-5 this was prevented by the melt-water interaction.

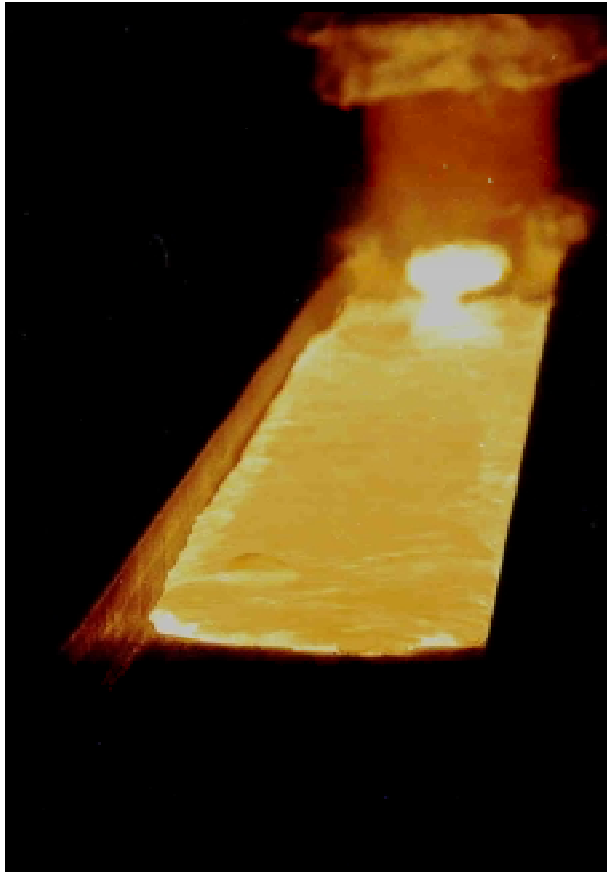


Figure 12: Melt surface photo in mini-KATS-5 at 5.9 s after start of spreading

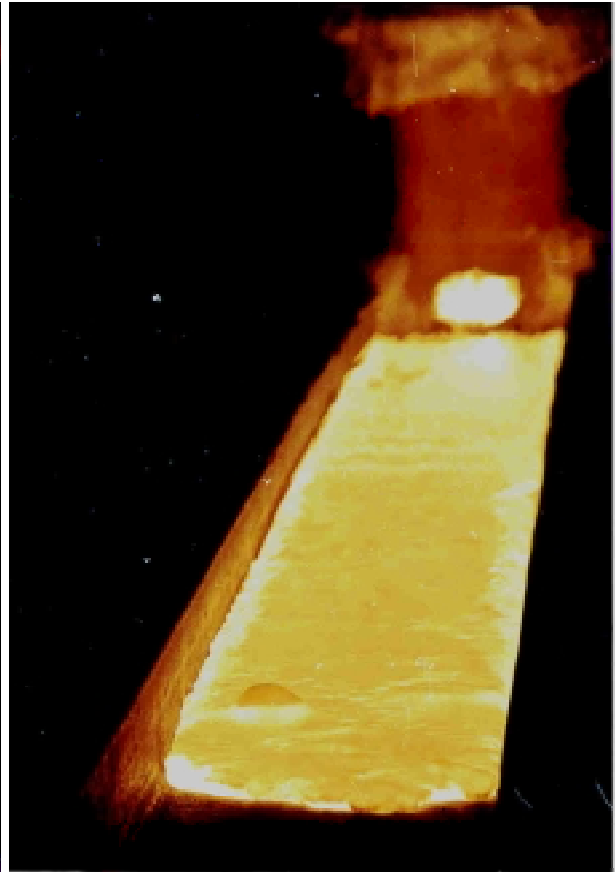


Figure 13: Melt surface photo in mini-KATS-5 at 6.8 s after start of spreading

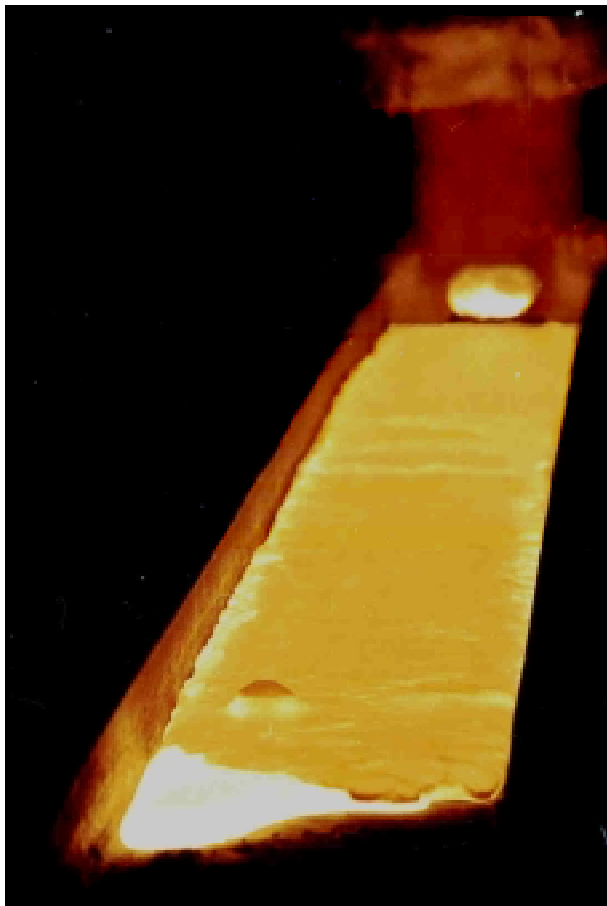


Figure 14:  
Melt surface photo in miniKATS-5 at 8.6 s after start of spreading

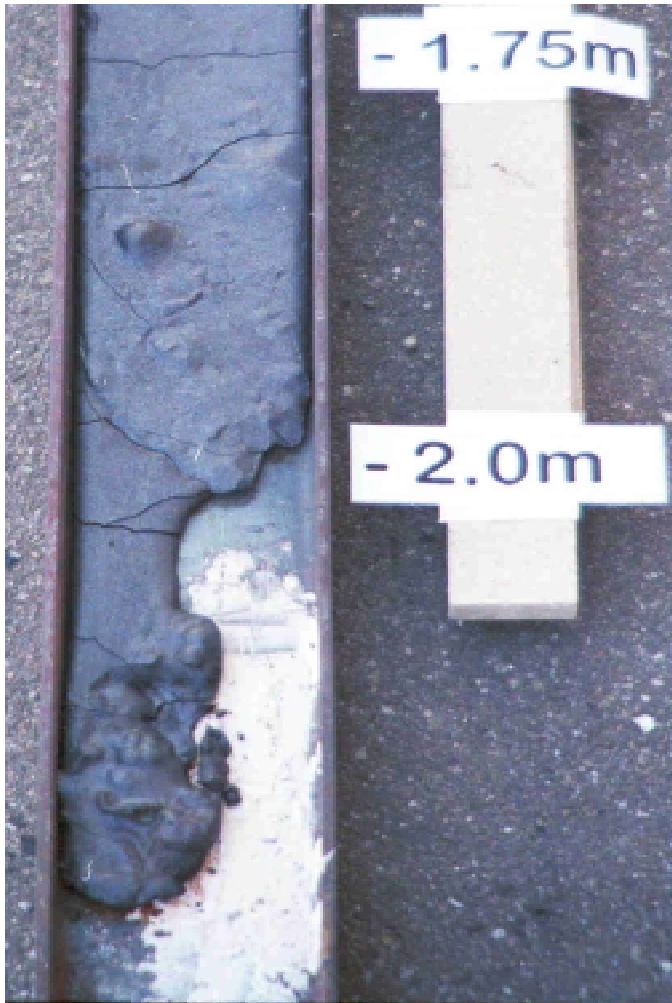


Figure 15: Shape of the solidified melt after the test

#### 4.5.2 Post-test examination

The colour of the melt (dark grey) is similar to that in miniKATS-4. The crust surface is again very smooth. In the middle of the channel, especially between 0 m and 1.7 m, some sort of vortex structure is visible. A structure of larger crystals near the melt outlet can be observed. The crust that stopped at 2.0 m caused a small vertical step in the solidified melt. The thickness at the very front cannot be measured, because the interaction between the melt and the filler material left the crust very uneven. But nearby to this location a thickness of 8 - 9 mm can be found. Up to 1.8 m the thickness in the middle of the channel is very low, only 6 – 6.5 mm, the crusts are higher near the sidewalls (10-12 mm).

### 4.5.3 Summary

The spreading was also very quick, continuous and smooth like in miniKATS-2, -3 and -4. The surface crust floats on a cushion of hot melt. Crust formation did not hinder spreading because melt flow continued beneath the crust.  $T_{\text{crust}}$  seems to be in the same range as in miniKATS-4. Spreading is quite similar to miniKATS-4 up to 5 s. The final spreading length and therefore average melt thickness are slightly different.

## 5 Discussion of observed spreading behaviour

The miniKATS-2 to -5 tests are quite similar concerning both the time-dependent spreading (Figure 6) and the visible spreading phenomena. MiniKATS-1, on the other hand, differs from the others in many aspects like transient spreading, total spreading length, slug thickness and the behaviour of early crust formation. This raises the question for the principal difference between miniKATS-1 and miniKATS-2 to -5. The main difference in the initial conditions is the melt temperature at the onset of spreading in relation to the solidification temperature or the liquidus temperature. This temperature range was smallest for miniKATS-1, with an initial temperature of 2015°C and first crusts forming at 1950°C, while tests miniKATS-2, -3, -4 and -5 had initial temperatures 200°C to 300°C above the observed  $T_{\text{crust}}$  (Table 3).

In detail, the following comments are made separately for the cases of strongly superheated melts and melts with temperatures near liquidus.

### 5.1 Spreading of strongly superheated melts (miniKATS-2 to -5)

In the case of a steady and evenly progressing flow of the melt from the iron swamp over the small dam onto the spreading channel, spreading can be described by an almost constant velocity of the melt front, as long as fresh melt is supplied from the reaction crucible. This can be seen in Figure 6. The melt front does not stop abruptly at the end of pouring but slows down steadily. From this behaviour one can assume that the spreading of superheated melts can be described by a continuity equation as follows:

$$h(t) = \frac{\dot{V}(t)dt}{w \cdot l(t)}$$

$h(t)$  = average melt height, time-dependent

$\dot{V}(t)$  = inflow rate

$w$  = width of channel, a constant

$l(t)$  = spreading length, time-dependent

The volumetric inflow rate could not be measured but was calculated as described in chapter 3.5 (Figure 5). These calculations are in good agreement with the observed total pouring duration of each test (Table 1), and therefore seem to be realistic values. So, with the calculated inflow rate, the channel width and the observed melt front position, the history of the average melt height was calculated. The following diagram, Figure 16, shows the results of these calculations for miniKATS-2 to miniKATS-5.

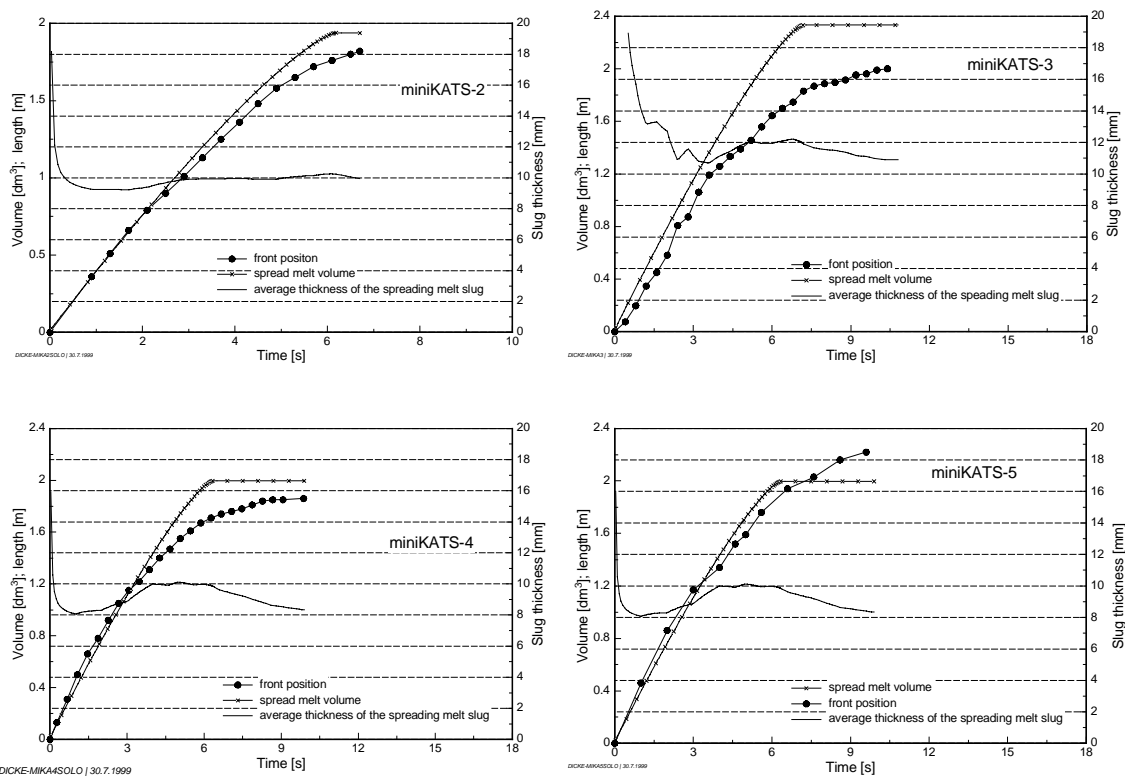


Figure 16: Calculated transient melt heights in tests miniKATS-2 to -5

After a short time the calculated melt height  $h(t)$  reaches an asymptotic value, very close to the minimum value  $h_{\min}$ ,  $h(t) \sim \text{const} \sim h_{\min} = 9.3 \text{ mm}$ , which adjusts due to the balancing of the surface tension and gravitation pressures, see chapter 2. In all

tests this height was found from the melt outlet to the final spreading distance within a margin of  $\pm 2$  mm. From this finding and the equation above, the front velocity  $v$  can be calculated:

$$v = \frac{dl(t)}{d(t)} = \frac{\dot{V}}{h_{\min} \cdot w} \quad \text{with } v \sim \dot{V}$$

The spreading stops if  $\dot{V} = 0$ . This is essentially in agreement with experimental observation (see Figure 6).

Surface crusts begin to form at the leading edge and grow in opposite direction to the melt flow. Furthermore, from the video recording and infrared film one can clearly observe that the crusts begin to grow near the sidewalls and proceeds towards the center of the channel. A combined flow pattern is built up in the form of a fishbone.

### **Summary:**

In these cases of highly superheated oxide melts, the spreading is controlled by the surface tension, crust formation has essentially no influence on the spreading. Because of the high melt temperature the bottom crust is thin and therefore has small influence on spreading. Surface crusts are floating on top of the spreading melt in the first few seconds, they have practically no influence on spreading, and sticking to the channel walls only near the end of spreading.

## **5.2 Spreading of melts with temperatures near the liquidus temperature (miniKATS-1)**

The initial melt temperature in test miniKATS-1 was close to or even below the liquidus temperature, Table 3. The spreading velocity was considerably lower than in the four other tests. As in section 5.1 for highly superheated melts, also in this case an analysis has been done to evaluate the time dependent average melt height. The inflow rate  $\dot{V}(t)$  is calculated using the Torricelli law (chapter 3.5) and the transient spreading length  $l(t)$  is from video recordings. Figure 17 shows the result of this calculation. Within less than a second the melt height rises to 22 mm. This accumulation of melt is required to raise the gravitational pressure sufficiently to overcome the retarding effects of high viscosity and crust formation and promote spreading during pouring. During further spreading the calculated average melt height is decreasing

steadily to about 15 mm. Post experiment investigation of the oxide slug show a height distribution ranging from 25 mm at the melt outlet near the dam to 10 mm at the leading edge front. The averaged value agrees with the calculated one.

From the beginning of spreading a considerable fraction of the melt (increasing in time) is immobilised in the bottom crust and after ~4 s (still during pouring) in sticking surface crusts. If the melt height at the front is assumed to correspond to  $h_{\min}$  (~9.5 mm, post experiment measurements of the leading edge after immobilisation shows indeed this crust height), the melt stored in crusts can be determined from the difference between inflow and meltfront flow, Figure 17.

$$\dot{V}_{crust} = \dot{V} - v \cdot h_{\min} \cdot w$$

Because the immobilised fraction of the melt is not available for spreading, this explains why the spreading length in miniKATS-1 is only ~ 1 m compared to ~2 m in the other tests. About half of the original pouring rate is transformed into an early freezing crust.

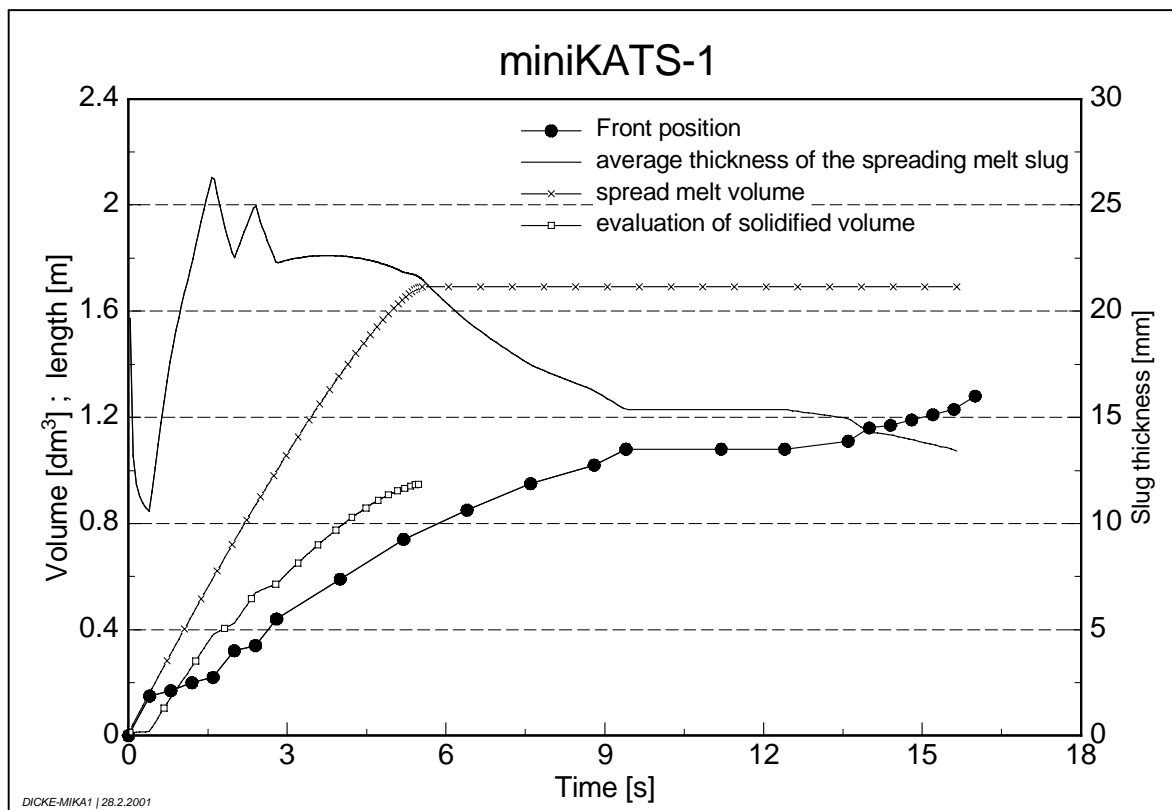


Figure 17: Calculated transient melt heights in miniKATS-1

**Summary:**

Two observations that are considered to be important for an understanding of spreading should be mentioned:

- ◆ Whereas at the upper surface of the spreading melt rather stable crusts are formed, at the meltfront at most locally weak skins but no stable crusts are observed. This is probably due to a continuous melt renewal caused by the formation of the bottom crust. Tentatively it is assumed that stable crusts can be formed at the melt front only if the bulk temperature there has dropped to  $\sim T_{50\%}$ .
- ◆ Occasionally, due to crust breakup, crust sticking or other effects, the temperature in the interior of the melt near the front and at the time of stop of spreading could be observed. (Table 4).

Table 4: Comparison of the melt front bulk temperature at immobilisation to the initial temperature

<b>Test</b>	<b>Bulk melt temperature (°C) initial</b>	<b>Bulk melt temperature (°C) Melt front, end of spreading</b>
MiniKATS-1	2015	1950 – 1990
MiniKATS-2	>> 2130	> 2100
MiniKATS-3	≥ 2130	-
MiniKATS-4	≥ 2130	> 1900
MiniKATS-5	≥ 2130	≥ 2130

From Table 4 it can be seen that even after ~10 s spreading over distances of up to 2 m the bulk temperature is still very near to the initial melt temperature and in mini-KATS-2 to –5 definitely still well above the liquidus. This is mainly due to the good thermal insulation of the crusts.

### **5.3 Comparison of spreading behaviour in miniKATS-2 to -5, miniKATS-1 and the large KATS tests**

Although crust formation is observed during the spreading of the superheated melts in miniKATS-2 to -5, it has essentially no influence on the spreading. The melt spreads evenly to  $h_{\min}$  (~9-10 mm) determined by the equation between gravitational and surface pressures.

In miniKATS-1, on the other hand, the initial melt temperature was near or even below the liquidus temperature. High viscosity and early massive crust formation hinders spreading and causes a large fraction of the available melt to be immobilised in crusts. Compared to the superheated melts, the spreading length is remarkably smaller and the average height of the slug correspondingly higher. The slug height decreases from ~ 25 mm at the channel entrance to ~10 mm at the melt front. The surface of the frozen slug is very uneven.

In the large KATS tests [6] [7] ~170 kg of oxide melt is spread in ceramic channels over distances between 6 and 12 m in several ten seconds. Depending on the melt superheat and the pouring rate, slug thickness between 30 and 60 mm and at the melt front single fingers with a thickness of ~10 mm are observed. Because the slug thickness is, as in miniKATS-1, much higher than  $h_{\min}$  it is concluded, that in these tests spreading is also strongly influenced by immobilisation of a large fraction of the available melt by crust formation.

## 6 Conclusions

In this series of five miniKATS tests small amounts of oxide melts (5 – 7 kg) with different initial temperatures have been poured on a channel and spread over distances between 1 and 2 m in about 10 s. Especially the phenomena at the melt front have been studied with the goal to understand what finally causes the stop of spreading.

The most important results of this study are:

- ◆ Spreading of the superheated melts in miniKATS-2 to –5 is stopped by the surface tension (although crusts are formed during spreading).
- ◆ Spreading of the miniKATS-1 melt with a temperature near liquidus is, besides surface tension effects, strongly influenced by melt immobilisation due to crust formation. Melt immobilisation seems to be also important in the large KATS spreading tests.
- ◆ Whereas at the upper surface of the spreading melt, pretty fast stable crusts are formed, directly at the meltfront no stable crusts have been observed.
- ◆ Mainly due to the good thermal insulation by the crusts at the boundaries, the interior of the spreading melt stays for long times and over large spreading distances near to the initial temperature.

## 7 Literatur

- [1] H. Alsmeyer et al., "Studies on the Core Melt Retention Concepts for the EPR", Proc. SFEN/KTG Conf. On the EPR Project, Strasbourg, November 1995, p.204
- [2] H. Alsmeyer et al., "Ex-Vessel Melt Behaviour in the EPR", Proc SFEN/KTG Conf. On the EPR Project, Cologne, October 1997, p. 161
- [3] R. Wittmaack, "Numerical Simulation of Corium Spreading in the EPR with CORFLOW", Proceedings of the OECD Workshop on Ex-Vessel Debris Coolability, Karlsruhe, 15-18 November 1999, FZKA 6475, May 2000, pp 201-211
- [4] J.J Foit, A. Vesper, "Spreading with Variable Viscosity. CORFLOW Validation and Analysis of KATS Experiments", Proceedings of the OECD Workshop on Ex-Vessel Debris Coolability, Karlsruhe, 15-18 November 1999, FZKA 6475, May 2000, pp 212-220
- [5] B. Spindler et al., "Assessment of THEMA Code against Spreading Experiments", Proceedings of the OECD Workshop on Ex-Vessel Debris Coolability, Karlsruhe, 15-18 November 1999, FZKA 6475, May 2000, pp 221-234
- [6] G. Engel et al., "KATS Experiments to Simulate Corium Spreading in the EPR Core Catcher Concept", Proceedings of the OECD Workshop on Ex-Vessel Debris Coolability, Karlsruhe, Germany, 15-18 November 1999, pp. 148-155
- [7] B. Eppinger et al., "Simulationsexperimente zum Ausbreitungsverhalten von Kernschmelzen: KATS-8 bis KATS-17", Wissenschaftlicher Bericht FZKA 6589, Forschungszentrum Karlsruhe, Germany, 2001
- [8] Ch. Adelhelm, IMF I, Chemische Analytik, Analysenzertifikate, private communication, October 1998
- [9] S. Schmidt-Stiefel, private communication, December 1998
- [10] W. Bohl, "Technische Strömungslehre", Vogel-Verlag, 4.Auflage, 1980